# AgriChrono: A Multi-modal Dataset Capturing Crop Growth and Lighting Variability with a Field Robot

Jaehwan Jeong<sup>1,2</sup>, Tuan-Anh Vu<sup>2</sup>, Mohammad Jony<sup>3</sup>, Shahab Ahmad<sup>3</sup>, Md. Mukhlesur Rahman<sup>3</sup>, Sangpil Kim<sup>1</sup>, and M. Khalid Jawed<sup>2\*</sup>

<sup>1</sup> Korea University <sup>2</sup> UCLA <sup>3</sup> North Dakota State University

## **Abstract**

Advances in AI and Robotics have accelerated significant initiatives in agriculture, particularly in the areas of robot navigation and 3D digital twin creation. A significant bottleneck impeding this progress is the critical lack of "inthe-wild" datasets that capture the full complexities of real farmland, including non-rigid motion from wind, drastic illumination variance, and morphological changes resulting from growth. This data gap fundamentally limits research on robust AI models for autonomous field navigation and scene-level dynamic 3D reconstruction. In this paper, we present AgriChrono, a modular robotic data collection platform and multi-modal dataset designed to capture these dynamic farmland conditions. Our platform integrates multiple sensors, enabling remote, time-synchronized acquisition of RGB, Depth, LiDAR, IMU, and Pose data for efficient and repeatable long-term data collection in real-world agricultural environments. We successfully collected 18TB of data over one month, documenting the entire growth cycle of Canola under diverse illumination conditions. We benchmark state-of-the-art 3D reconstruction methods on AgriChrono, revealing the profound challenge of reconstructing high-fidelity, dynamic non-rigid scenes in such farmland settings. This benchmark validates AgriChrono as a critical asset for advancing model generalization, and its public release is expected to significantly accelerate research and development in precision agriculture. The code and dataset are publicly available at: https: //github.com/StructuresComp/agri-chrono

## 1. Introduction

Precision agriculture has emerged as a critical field where the rapid advancement of AI and Robotics is accelerating significant new initiatives. Notably, Agricultural Digital Twins (ADT) are gaining significant traction [6, 21, 33], which leverage data collected by autonomous robots [13,



Figure 1. Overview of the *AgriChrono* field-scale data collection framework. **Top**, a real-world outdoor agricultural field used for data acquisition. **Middle left**, user interface for remote robot control and data collection. **Bottom left**, robotic platform with multiple sensors for field data collection. **Bottom right**, time-aligned multi-modal frame with RGB, Depth, and LiDAR data.

25] to create high-fidelity 3D models. These models serve as structural digital counterparts of physical farmland [28], enabling precise crop phenotyping and monitoring [25, 27]. This potential, however, is severely constrained by a fundamental bottleneck [8, 20], namely the lack of public datasets that adequately capture real-world agricultural complexities. To achieve effective autonomous navigation and accurate 3D reconstruction for phenotyping, it is essential to collect comprehensive data that reflects the continuous morphological changes of crops during their growth stages. This data must also account for all naturally occurring phenomena, such as the varying illumination caused by the sun's position and the dynamic movements of non-rigid crops, which can shift due to environmental influences like wind.

<sup>\*</sup>Co-corresponding Authors

Table 1. **Comparison of related agricultural datasets.** Existing datasets are typically focused on either robot-centric navigation or crop-centric phenotyping. *AgriChrono* dataset is uniquely designed to address both, providing Visual-Inertial Odometry (VIO) based pose for **Localization** while simultaneously capturing the entire crop **Growth Span** under four systematic **Illumination** conditions for phenotyping. Accordingly, we collected 175 sessions over one month using two Stereo Cameras and one LiDAR, culminating in this comprehensive, dual-purpose dataset, which results in a dataset of unprecedented scale (18 TB).

\* Synthetic dataset generated via simulation.

Dataset	Modalities	Localization	<b>Growth Span</b>	Illumination	Platform	Size
Rosario [29]	RGB, Depth, IMU, Pose	✓	Х	×	UGV	N/A
AgScan3D [18]	LiDAR, IMU, Pose	$\checkmark$	$\checkmark$	×	UGV	N/A
Terrasentia [4]	RGB, Depth, IMU, Pose	$\checkmark$	$\checkmark$	2	UGV	1 TB
PlantSegNet [39]	Geometry*	✓	$\checkmark$	4+	Simulation	N/A
BonnBeetCloud3D [23]	RGB, Pose	$\checkmark$	×	×	UAV	10 GB
MinneApple [7]	RGB	×	×	2	Handheld	3 GB
CRDLD [5]	RGB	X	×	4	UGV	1 GB
Agroscapes [26]	RGB	×	×	×	UAV, UGV, Handheld	9 GB
Crops3D [41]	RGB, LiDAR, SL	X	×	×	Fixed, Handheld	9 GB
NIRPlant [2]	RGB, Depth, NIR, LiDAR	X	×	4	Fixed	554 GB
AgriChrono	RGB, Depth, LiDAR, IMU, Pose	· 🗸	✓	4	UGV	18 TB

To address these gaps, we introduce AgriChrono, a robotic platform and in-the-wild, multi-modal dataset designed to reflect the complexity and diverse environmental variations of real agricultural scenes (Fig. 1). Our robotic platform features a highly modular design possessing significant extension potential and boasts field-proven stability, as validated by over a month of continuous operation. It ensures the time-synchronized acquisition of 4-view RGB, 2-view Depth, LiDAR, IMU, and VIO Pose. The data collection protocol was remotely managed via our customdesigned Web UI, enabling stable acquisition from distances exceeding 1,500 miles. Using this platform, we stably collected a multi-modal dataset over one month across three crop sites (Canola, Flax, and a Canola genotype variant). Notably, for Canola, data were acquired every day during its main growth period to capture continuous structural changes, and systematically collected at four specific times daily to account for color shifts caused by the changing position of the sun. Consequently, we successfully constructed a dataset totaling approximately 18 TB across 175 sessions.

We also introduce a new 3D reconstruction benchmark on non-rigid in-the-wild scenes based on the *AgriChrono* dataset, featuring seven scenarios (Lighting Variance and Morphological Change). Our evaluation reveals that state-of-the-art methods from the last three years exhibit low performance when faced with the complexities naturally occurring in open fields, particularly struggling with the dynamic movements and thin structures of non-rigid targets. This finding establishes *AgriChrono* as a necessary benchmark for measuring and bridging this real-world robustness gap. Ultimately, the dataset provides a vital tool to drive advancements in 3D reconstruction and the broader adoption of AI in precision agriculture.

The main contributions of this work are as follows:

- We developed a modular robotic platform for data collection, capable of remote hands-off operation via a customized Web-UI. This platform enabled the systematic and high-quality collection of multi-modal data (RGB, Depth, LiDAR, IMU, Pose) over a long term.
- We release the 18 TB AgriChrono dataset, which captures comprehensively the in-the-wild environment. The data was captured four illumination times daily during the crop's main growth period, documenting the continuous morphological changes within a complex natural setting.
- We introduce a new benchmark for 3D reconstruction methods, featuring seven scenarios designed to reflect complex, in-the-wild agricultural environments. This benchmark illustrates the significant challenges of reconstruction under such conditions and highlights the crucial role of the *AgriChrono* dataset in advancing research.

## 2. Related Work

## 2.1. Agriculture Datasets

Robot-centric Datasets for Navigation. Existing robot-centric datasets in agriculture primarily focus on localization and navigation benchmarks, such as Simultaneous Localization and Mapping (SLAM) and odometry. These datasets generally aim to provide robust trajectories by centrally utilizing localization sensors (like IMU, GNSS, and Odometry) and employing perception sensors (RGB-D and LiDAR) to understand the surrounding environment. Due to this purpose-orientation, these datasets have limitations in capturing fine-grained crop phenotyping information or dynamic environmental changes. For instance, Rosario [29] is temporally sparse, consisting of only six sequences recorded over two days. This fails to capture long-term environmental or crop changes. Although AgScan3D [18] col-

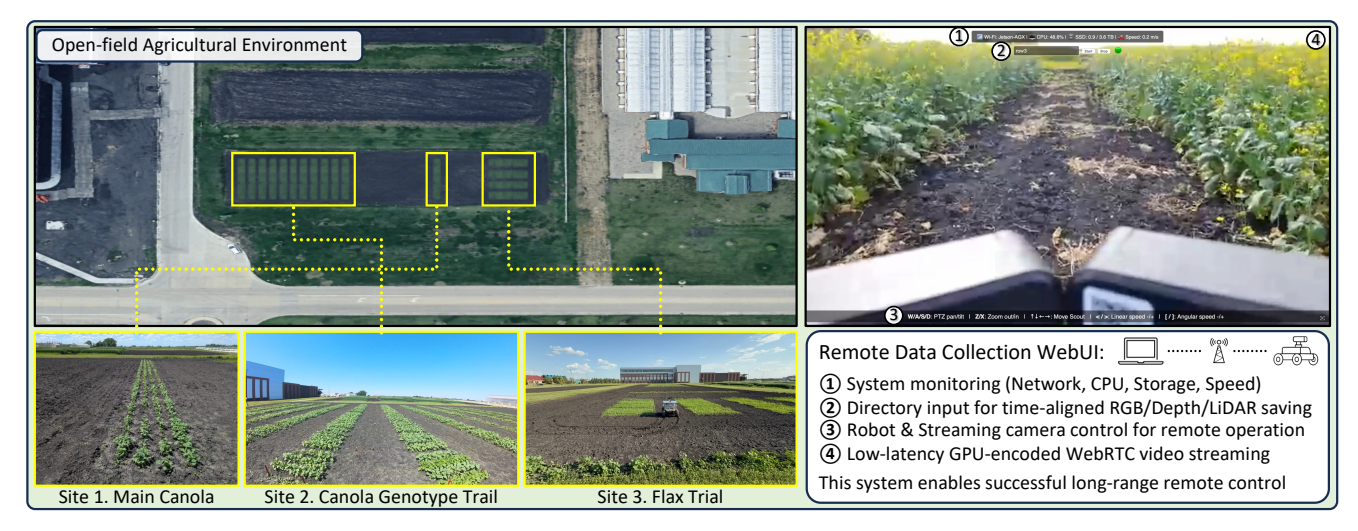


Figure 2. Data collection sites and the remote operation interface used during field trials. **Site 1**, main canola site used as the primary location for repeated data collection, capturing temporal changes in illumination and crop structure. **Site 2**, genotype trial site featuring diverse canola varieties, enabling the capture of morphological variation across crop types. **Site 3**, flax trial site composed of multiple plots with varying weed control strategies, providing structural diversity in a controlled multi-block layout. **WebUI**, remote interface supporting real-time system feedback, intuitive directory-based data saving, responsive robot and camera control, and low-latency teleoperation.

lected 64 sessions over 23 months, its collection was sporadic, aligning with major phenological stages (e.g., preflowering, post-harvest) rather than a continuous growth cycle, and it fails to address illumination variance. Similarly, Terrasentia [4] attempted to capture the growth span and illumination changes, but its collection frequency was sparse (twice per week), and its illumination categories were overly broad (e.g., sunny/cloudy).

**Crop-centric Datasets for Phenotyping.** The datasets in this group primarily target crop phenotyping, including tasks such as classification, segmentation, and 3D reconstruction. However, these datasets are predominantly captured in controlled environments, feature limited sensor modalities, and are based on single-session acquisition from fixed or handheld platforms. This static data characteristic limits scalability to real-world robotic systems that must perform autonomous data collection and phenotyping in vast, in-the-wild settings. For example, MinneApple [7] is constrained by its handheld acquisition method, which inherently limits the data volume, and only considers two broad illumination conditions. While CRDLD [5] utilized a UGV to capture field conditions, it consists of singlepass, RGB-only recordings, resulting in a small dataset of only 1 GB. Similarly, Agroscapes [26] employed diverse platforms but is also restricted to single-pass, RGBonly data. Datasets like Crops3D [41], which offer multimodality (RGB, LiDAR, SL), still rely on fixed tripods or handheld capture. Finally, NIRPlant [2] achieves highfidelity 3D modeling but is object-centric, was captured in a controlled lab setting, and fails to capture the crop's full growth span. Aerial (UAV-based) datasets, such as BonnBeetCloud3D [23] and Growliflower [12], provide georeferenced poses but are typically restricted to top-down or high-angle RGB data. This perspective inherently occludes critical phenotyping features, including vertical crop structure, leaf overlap, and stem characteristics. Moreover, they suffer from temporal limitations; BonnBeetCloud3D does not cover the full growth span, and Growliflower's collection was limited to only once per week.

In summary, current datasets show a clear trade-off. Robot-centric datasets are suitable for autonomy tasks such as SLAM and navigation, but they lack the detailed information required for phenotyping. Conversely, crop-centric datasets offer this detail but struggle with scalability for autonomous data collection in large, open fields. Importantly, both types have largely overlooked two core challenges of real-world environments: (i) the ongoing structural changes of growing crops and (ii) the wide range of color variations caused by daily lighting changes. These limitations may affect the ability to create models that generalize well; therefore, we present a new dataset, *AgriChrono*, designed to address both of these challenges.

### 2.2. Neural Rendering Methods

**NeRF-based methods.** Neural radiance fields (NeRFs) model a continuous 5D volumetric radiance field from 3D position and viewing direction. We use Nerfstudio [35] as both a baseline and unified training/evaluation framework, with Zip-NeRF [1] reducing aliasing in grid-based NeRFs via cone tracing and multi-resolution grids, NeRF on-thego [31] employing uncertainty-driven modeling to handle moving distractors and transient appearance, and Tetra-NeRF [14] representing NeRFs on tetrahedral meshes to enable efficient sampling and rendering of complex geometry.

**3DGS-based methods.** The original Gaussian Splatting method [9] represents scenes as anisotropic 3D Gaussians rendered via screen-space splatting, achieving NeRF-level image quality with real-time rendering and fast training, and serves as our main explicit baseline. GS-W [40] and WildGaussians [16] extend 3DGS to in-the-wild data by modeling dynamic appearance, occlusions, and illumination, while Taming 3DGS [22] and gsplat [38] improve efficiency via budgeted densification and optimized CUDA rasterization. For large scenes, Scaffold-GS [19] organizes local neural Gaussians around sparse SfM anchors, Octree-GS [30] imposes an octree level-of-detail hierarchy for scalable view-dependent rendering, and H3DGS [10] introduces a hierarchical multi-scale 3D Gaussian representation for real-time rendering of very large datasets. 3D-GRT [24] replaces rasterization with BVH-based ray tracing to support semi-transparency and shadows, while 3DGUT [37] uses an unscented-transform approximation to handle non-linear camera models and secondary effects in real time. Probabilistic and geometry-focused variants, such as MCMC [11], treat Gaussians as samples from a radiance distribution, replacing heuristic densification with Langevin dynamics and principled relocalization for better control over model size and initialization. PGSR [3] emphasizes geometry, enabling efficient mesh or surface extraction for phenotyping traits (e.g., height, canopy volume).

Encompassing implicit volumetric, explicit geometry-aware, and probabilistic representations, these NeRF and Gaussian baselines are benchmarked on the *AgriChrono* dataset, which embodies in-the-wild complexity, enabling a systematic comparison for agricultural phenotyping.

## 3. Platform and Protocol

## 3.1. System Architecture

Robotic Platform Design. The *AgriChrono* platform is a field robot designed for long-term remote data collection in outdoor agricultural environments. Its modular design facilitates the integration of diverse sensors and ensures future expansion capability. As shown in Fig. 3, the system is built on the AgileX Scout 2.0 Unmanned Ground Vehicle (UGV), integrating a tiered sensor suite, an onboard compute unit, and a wireless communication module.

At the bottom tier, the Livox Mid-360 LiDAR was installed. This placement was designed to effectively capture the early growth stage (low height) of the crops, considering the model's asymmetric vertical field of view (FoV) specification ( $-7^{\circ}$  to  $+52^{\circ}$ ). Furthermore, the LiDAR was positioned at the front to prevent occlusion by the robot's wide top panel. Since the upper vertical FoV beyond  $+52^{\circ}$  is inherently unusable, this configuration offers the advantage that the subsequent installation of other sensors on the upper tiers will not impair the LiDAR's performance.

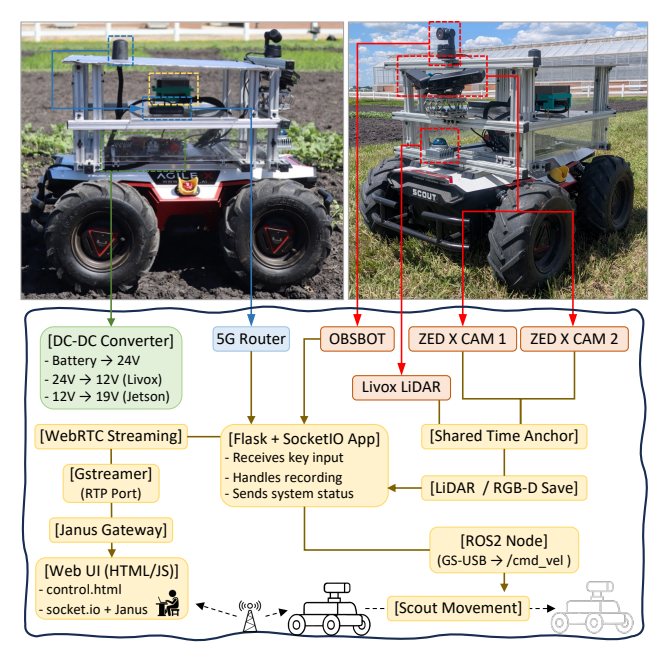


Figure 3. System diagram of the *AgriChrono* platform, showing the hardware configuration segmented into three modular tiers mounted on a UGV: The first tier houses the DC converter and LiDAR; the second tier contains the Edge Device, 5G Router, and two stereo cameras; and the third tier holds the antennas and the PTZ camera for robot control.

The middle tier consists of two ZED X (4mm lens) stereo cameras mounted on vibration-isolating and tilt-adjustable heads. The cameras are positioned with a 130° outward angle between them, yielding a 10° overlap and a combined 150° horizontal FoV for wide-baseline, multi-view Stereo RGB-D capture. Furthermore, a 3-axis flex tilt head was utilized for angle adjustment according to crop growth, and a Vibration Isolator was used to dampen high-frequency vibrations induced by the LiDAR and the robot itself.

The top tier features an OBSBOT camera with PTZ, which covers the forward, lateral, and downward directions, enabling intuitive awareness of the robot's surroundings and facilitating efficient remote teleoperation. All control and data acquisition are performed over a 5G Router with an omnidirectional antenna, maintaining stable communication during locomotion. The system features thermal protection through a sun-shielded top panel and is enclosed in a custom aluminum-acrylic chassis, ensuring robustness for prolonged operation on uneven farmland.

Modular Software Stack. The software stack is modular and runs on a Jetson AGX Orin 64GB embedded system. Robot control is managed via a ROS 2 Humble workspace that supports CAN-based teleoperation. For data logging, a dual-camera ZED logger captures temporally synchronized RGB-D recordings in the proprietary compressed file format, .svo2, alongside per-frame IMU data. Concurrently, a custom C++ module logs LiDAR point clouds and

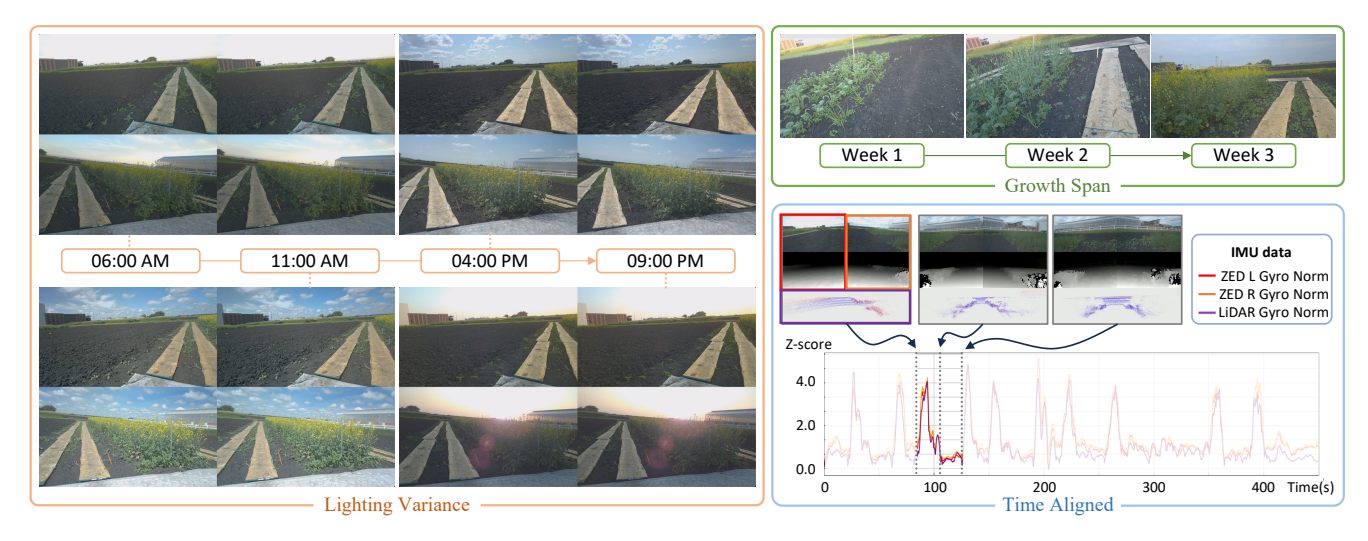


Figure 4. Visualization of dataset properties. (i) **Lighting Variance**: RGB frames of the same scene at four times of day, showing natural illumination changes. The top two images are from the left stereo camera, and the bottom two are from the right stereo camera. (ii) **Growth Span**: Weekly progression (Week 1–3) of the same crop row, highlighting canola growth and structural change. (iii) **Time Aligned**: Gyroscope magnitude (L2 norm) from IMU data of two ZED cameras and the LiDAR, Z-score normalized to verify cross-sensor alignment.

IMU data in a binary format. Sensor synchronization is ensured through a shared sync\_time.txt file generated at the start of each session, guaranteeing consistent temporal alignment across all modalities. This compressed file storage method significantly reduced I/O load and enabled the efficient storage of a large volume of data. For remote operation, a WebRTC-based streaming module (Janus Gateway + GStreamer) delivers low-latency video feeds by optimizing the encoder and bitrate. Simultaneously, the customized Flask-based browser UI, depicted in Fig. 2, enables teleoperation, PTZ control, and system diagnostics. Additional system utilities include boot-time hardware initialization to prevent interface conflicts, automatic reporting of IP and network status via email, and a fail-safe mechanism that continuously monitors the network connection and immediately halts robot operation if the session is lost, ensuring safe deployment in unattended field scenarios.

Data Collection Schedule. Data were collected over one month, structured into two distinct phases based on the crop's growth activity. During Phase 1 (July 2–21), when growth was active, sampling was performed systematically four times daily, seven days a week, specifically at 6:00 AM (sunrise), 11:00 AM (high sun), 4:00 PM (low sun), and 9:00 PM (sunset). This schedule ensured the capture of varying illumination and morphological changes, as verified in Fig. 4. In Phase 2 (July 22–August 1), as growth slowed toward maturity, sampling frequency was reduced to twice per week. The main canola site was scanned twice (clockwise and counterclockwise) to capture both the front and rear views of the crops. In contrast, the two auxiliary sites were sampled throughout the study period, with data collected once or twice weekly on selected days.

Field Conditions. Data collection was performed across three field sites, as shown in Fig. 2. The entire process was suspended only during rainfall. To ensure continuous operation and robot mobility, wooden planks were placed along the traversal path to secure stable operation even on wet soil. Field Site Configurations. The dataset was collected from three distinct field sites, each contributing complementary variability. Site 1 served as the primary data collection site, composed of a single canola variety (InVigor L340PC), and one block with four rows spanning 50 ft × 3 ft. This site enabled consistent tracking of temporal appearance changes under varying growth stages and lighting conditions. Site 2 consisted of 11 blocks, each configured as a 44 ft  $\times$  3 ft plot and assigned a unique canola genotype. This layout was designed to capture morphological and structural variation across genotypes. Site 3 focused on a different crop, flax (Gold ND), and was organized as a  $4 \times 4$  grid of plots (8 ft  $\times$  3 ft each), totaling 16 plots. In contrast to the previous sites, this configuration introduced additional structural diversity through both the crop type and its spatial arrangement. Together, these three sites offer complementary variation across temporal, morphological, and spatial dimensions, forming a robust foundation for training models that can generalize across diverse field scenarios.

## 4. Dataset Analysis

## 4.1. Dataset Properties

The dataset consists of time-synchronized multi-modal samples, each comprising RGB images, depth maps, Li-DAR scans, IMU readings, and 7-DOF Pose. The RGB modality (from two stereo cameras) provides four  $1920 \times 10^{-2}$ 

Table 2. Statistics of the *AgriChrono* dataset collected at three field sites, detailing the number of recording sessions, total duration, average frame rate, total number of time-synchronized multi-modal samples (each comprising four RGB images, two depth maps, Li-DAR scans, IMU, and Pose), and the overall data volume.

Site	# Sessions	FPS	<b>Duration</b> (s)	# Samples	Size
Site 1 <sub>CW</sub>	80	14.7	18,834	276,656	6.8 TB
Site $1_{\text{CCW}}$	80	14.7	19,098	282,919	6.9 TB
Site 2	7	13.1	10,235	129,088	3.2 TB
Site 3	8	14.6	2,879	42,097	1.1 TB
Total	175	14.3	51,046	730,760	18 TB

1080 images, covering a 150° horizontal FoV. Two depth maps, aligned to the left cameras, are also included in each sample, computed using the ZED SDK's neural depth estimation mode. The 7-DoF pose information is derived from time-synchronized RGB and IMU data captured by two separate ZED units. The individual VIO output from each unit serves as the Ground Truth camera pose for its respective image, while fusing these two time-synchronized VIO outputs yields a highly robust robot trajectory (detailed in the Supplementary Material). LiDAR point clouds are available in both a forward-facing 150° subset and the full 360° scan. IMU measurements are provided for all sensing units. Each stereo camera system records three-axis accelerometer and gyroscope data, while the LiDAR unit records three-axis gyroscope and single-axis accelerometer data. All modalities share a standard timestamp system, with accuracy confirmed by the close alignment of gyroscope measurements across all three sensors, as shown in Fig.4.

In total, as summarized in Table 2, the *AgriChrono* dataset comprises 160 sessions at Site 1, with the remaining sites yielding 7 and 8 sessions, respectively. The entire dataset contains 730,760 paired samples recorded at an average rate of 14.3 FPS over approximately 51,046 seconds, resulting in 18 TB of extracted data (roughly 3 million individual images, counting RGB alone). To ensure consistent crop coverage across all sessions, the camera's vertical tilt was adjusted once during the collection period to accommodate changes in crop height.

#### 4.2. Dataset Structure

The dataset is organized as illustrated in Fig. 5. Depth data are stored in both .npz and .png formats. The RGB data consist of four .png image pairs, acquired from the left and right sensors of each stereo camera. LiDAR point clouds are saved in .ply format within two separate directories corresponding to the different FoV. Two accompanying \*\_info.csv files provide the IMU measurements and timestamps for each synchronized sample within the session. Additionally, pose\_info.csv provides the frame-synchronized 7-DoF pose information obtained from the VIO of each of the two cameras.

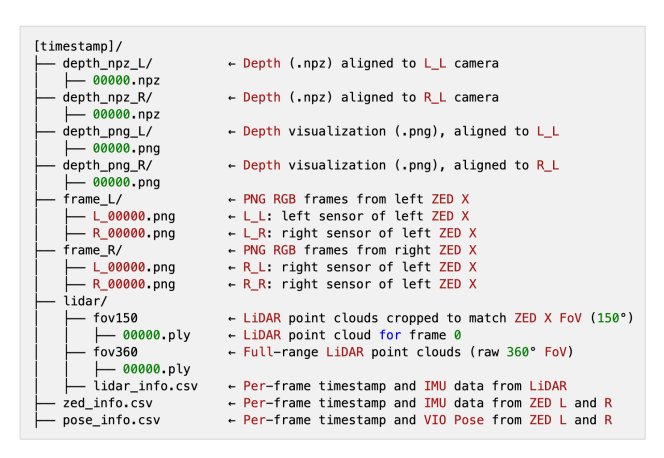


Figure 5. Public release format of the AgriChrono dataset

## 5. Benchmark

We present a novel benchmark for evaluating 3D reconstruction in complex in-the-wild agricultural environments using *AgriChrono* dataset. It comprises seven scenarios spanning four distinct Lighting Variance and three Morphological Change conditions. We evaluate 12 Gaussian Splatting-based methods among the state-of-the-art 3D reconstruction techniques from the last three years, as shown in Table 3 and Fig. 7, and provide NeRF baselines in the Supplementary Material for comprehensive comparison.

## 5.1. Benchmark Settings

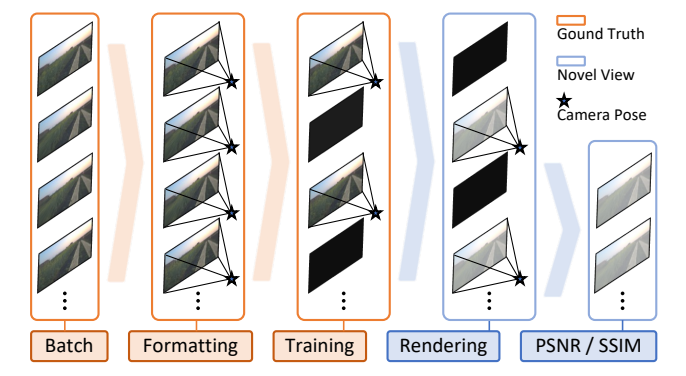


Figure 6. For each scenario, a batch of 400 images (at ~9cm intervals) is formatted with its corresponding Depth and Pose information. This batch is used for pose estimation, split into training and test sets in a 7:1 ratio, and subsequently used for model training and metric evaluation.

As shown in Table 3, the benchmark evaluates two core challenges across seven scenarios. The first, Lighting Variance, consists of four scenarios using Day 19 captures at four distinct times (6:00 AM, 11:00 AM, 4:00 PM, 9:00 PM) to assess robustness to lighting changes. The second, Growth Span, comprises three scenarios captured at 06:00 AM across weekly growth stages (Day 6, Day 13, Day 20) to evaluate robustness under temporal morphological change over the crop lifecycle.

Table 3. Novel View Synthesis Benchmark on AgriChrono dataset (Site  $1_{CCW}$ ) evaluating performance under Lighting Variance and Growth Span. The benchmark was conducted on 12 state-of-the-art 3D reconstruction methods from the last three years, which were evaluated across a total of seven distinct conditions. The quantitative evaluation performance is reported using the PSNR and SSIM. Overall, the observed performance degradation underscores the fundamental challenge of applying existing 3D reconstruction techniques to in-the-wild, non-rigid agricultural scenes, resulting in generally suboptimal reconstruction quality.

Condition			Light	Lighting Variance (Day 19)					Growth Span (6 AM)						
Condition	06:00	) AM	11:00	) AM	04:00	) PM	09:00	09:00 PM		Day 6		Day 13		Day 20	
Method	PSNR↑	SSIM↑	PSNR↑	SSIM↑	PSNR↑	SSIM↑	PSNR↑	SSIM↑	PSNR↑	SSIM↑	PSNR↑	SSIM↑	PSNR↑	SSIM↑	
3DGUT [37]	26.433	0.6915	22.860	0.5488	24.147	0.5906	27.813	0.7134	23.706	0.5130	24.856	0.5597	25.858	0.6477	
Octree-GS [30]	28.451	0.8009	24.402	0.7044	25.593	0.7269	29.716	0.8092	26.211	0.7098	27.669	0.7545	27.677	0.7771	
gsplat [38]	27.242	0.7637	23.740	0.6630	25.012	0.6882	28.714	0.7827	25.431	0.6348	26.730	0.6977	26.922	0.7355	
3D-MCMC [11]	27.053	0.7194	23.385	0.5886	24.667	0.6281	28.180	0.7370	24.556	0.5566	26.134	0.6349	26.357	0.6795	
WildGaussians [16]	7.298	0.4037	11.498	0.3847	11.022	0.4061	8.158	0.4506	23.057	0.5129	24.422	0.5812	11.655	0.5140	
GS-W [40]	20.338	0.6593	17.946	0.5033	20.337	0.5588	22.819	0.7015	23.474	0.5186	23.616	0.5885	19.967	0.5889	
H3DGS [10]	<u>27.990</u>	0.7939	24.412	0.7076	<u>25.488</u>	<u>0.7204</u>	<u>29.330</u>	0.8042	25.473	0.6680	<u>27.260</u>	0.7390	27.350	<u>0.7685</u>	
3DGRT [24]	26.702	0.7653	23.599	0.6616	24.733	0.6896	28.463	0.7828	25.317	0.6351	26.424	0.6986	26.301	0.7373	
Taming3DGS [22]	27.908	0.7756	24.342	0.6854	25.453	0.7012	29.179	0.7896	25.780	0.6533	27.241	0.7187	27.534	0.7495	
Scaffold-GS [19]	25.542	0.7403	21.193	0.6280	24.661	0.6739	27.770	0.7743	24.816	0.6427	25.286	0.6887	24.612	0.7032	
PGSR [3]	26.697	0.7429	23.673	0.6415	24.634	0.6610	28.277	0.7585	24.148	0.5459	25.236	0.6271	26.607	0.7122	
3DGS [9]	27.107	0.7717	23.950	0.6742	24.970	0.6932	28.788	0.7884	25.449	0.6449	26.891	0.7097	26.987	0.7420	

As shown in Fig. 6, each of the seven scenarios consists of a batch of 400 frames, curated to cover the entirety of Site 1 with a uniform spatial interval of ~9cm. Subsequently, each frame is structured in the COLMAP [32] format, using its corresponding RGB image (resized to 960 × 540), intrinsic camera parameters, a sparse 3D point cloud (sampled at 0.1% from Depth), and the extrinsic camera pose derived from VIO. For the Novel View Synthesis evaluation, each batch is split into 350 images for training and 50 for testing, and performance is evaluated using PSNR and SSIM.

A notable aspect is that our benchmark dataset provides reliable extrinsic poses in non-rigid dynamic environments, which traditional Structure-from-Motion (SfM) and recent learning-based methods, such as VGGT [36], typically fail to produce. This is enabled by the fact that the *AgriChrono* dataset was collected using a robot moving at a uniform velocity of 0.2m/s, with time-synchronized data at ~15 FPS. Furthermore, we utilize IMU data to generate highly reliable pose data, which is essential for this benchmark. A detailed analysis is provided in the Supplementary Material.

## 5.2. Benchmark Analysis

Table 3 summarizes novel view synthesis performance under *Lighting Variance* and *Growth Span*. Overall PSNR/SSIM values remain moderate, indicating that all methods struggle with substantial appearance changes and complex canopy geometry. Octree-GS [30] achieves the best average performance across almost all conditions, while H3DGS [10] and Taming3DGS [22] form a second tier with slightly lower scores. Lighting variation has a clear impact: reconstructions at 11:00 AM (harsh sunlight) are

Table 4. **Resource usage of Gaussian Splatting Baselines.** All methods were evaluated on an NVIDIA RTX 6000 Ada GPU using the NerfBaselines [15] framework.

Year	Method	Training Time	GPU Memory
2025	3DGUT [37]	7m Os	6,315 MB
2025	Octree-GS [30]	13m 23s	5,578 MB
2025	gsplat [38]	5m 15s	1,834 MB
2024	3D-MCMC [11]	4m 56s	4,512 MB
2024	WildGaussians [16]	1h 1m 28s	2,022 MB
2024	GS-W [40]	58m 32s	7,027 MB
2024	H3DGS [10]	38m 12s	8,602 MB
2024	3DGRT [24]	27m 52s	7,866 MB
2024	Taming3DGS [22]	4m 31s	6,016 MB
2024	Scaffold-GS [19]	8m 25s	4,785 MB
2024	PGSR [3]	7m 30s	4,770 MB
2023	3DGS [9]	6m 43s	4,665 MB

notably worse than those at 6:00 AM or 9:00 PM, indicating that current splatting methods handle soft, diffuse lighting better than intense, directional illumination. Along the growth axis, early-stage Canola (Day 6) is the hardest to reconstruct, likely due to its fine-scale structure and exposed soil. In contrast, performance improves as the canopy densifies, yet still falls short of typical indoor benchmarks.

Figure 7 provides qualitative examples for the top-five performing methods. A key observation is that, regardless of illumination time or growth week, all methods deviate from the ground truth in terms of delicate canopy reconstruction. Although Octree-GS [30] most closely preserves the overall appearance, the remaining baselines ex-

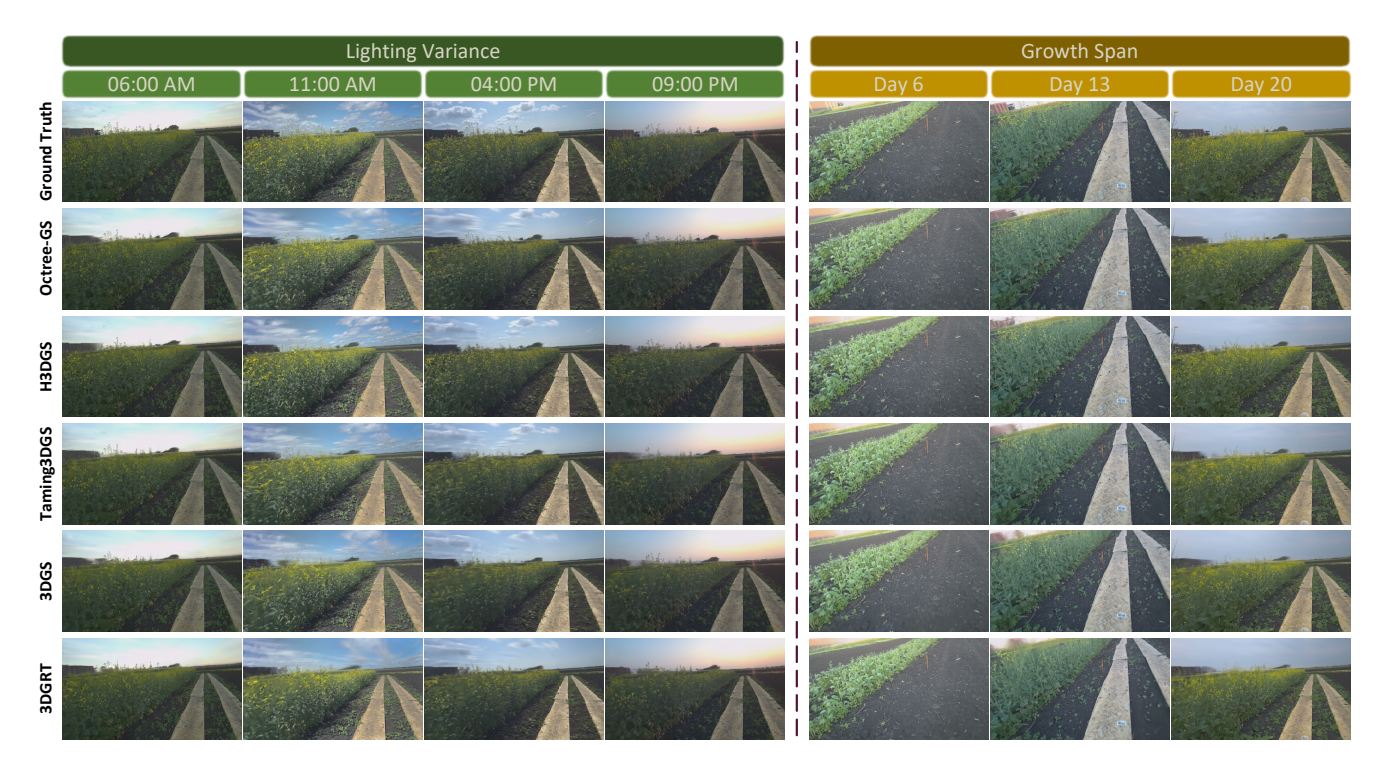


Figure 7. **Qualitative results** for the top five methods [9, 10, 22, 24, 30] from the *AgriChrono* benchmark table are presented in order. Although the rendered novel-view images appear superficially similar to the ground truth, a closer inspection reveals that the fidelity of the canopy reconstruction degrades in accordance with their quantitative scores. This consistent degradation highlights the failure of existing methods on non-rigid, scene-level data and validates our benchmark scores. This difficulty stems specifically from poor feature matching performance and the challenge of modeling the inherent geometric complexity of agricultural scenes. Zoom in for better visualization.

hibit more pronounced blur and inconsistencies on thin leaves and around the soil-canopy boundary, particularly under noon lighting and during the early growth stage. This aligns with the quantitative degradation observed in Table 3.

Table 4 reports training time and GPU memory on an NVIDIA RTX 6000 Ada. All methods train within one hour, but higher resource usage does not necessarily translate to better accuracy. Octree-GS [30] offers a favorable balance, combining top performance with moderate training time and memory. At the same time, fast baselines such as gsplat [38] and Taming3DGS [22] provide competitive results at a fraction of the cost. In contrast, several heavier methods consume substantially more resources without clear gains on *AgriChrono* benchmark, underscoring that architectures tuned on conventional datasets may not generalize well to in-the-wild agricultural scenes.

## 6. Conclusions

In this study, we introduce *AgriChrono*, a novel resource encompassing a custom robotic platform, its resulting 18TB multi-modal dataset, and a seven-scenario 3D reconstruction benchmark. Our dataset provides time-aligned RGB, Depth, LiDAR, IMU, and Pose data that captures long-term growth and four distinct lighting variations, fully re-

flecting the complexity of agricultural fields. Based on this, we present a novel benchmark composed of seven scenarios to evaluate 3D reconstruction in non-rigid, in-the-wild environments. This work provides a vital tool to drive advancements in 3D vision research and accelerate the broader adoption of AI in precision agriculture.

**Limitations and Future Work.** As shown in Table 2, our data collection faced challenges. While Sites 1 and 3 maintained a stable synchronization rate of ~15 FPS, yielding reliable pose information, Site 2 exhibited lower FPS values. This degradation, which affected pose accuracy, stemmed from thermal issues that occurred during prolonged operation. To address these limitations, our immediate future work involves refining the platform structure to mitigate thermal issues and developing software solutions for dynamic time-synchronization and global adjustment via RTK-GNSS. Separately, we will utilize the AgriChrono dataset & benchmark to develop robust 3D reconstruction methods for non-rigid agricultural scenes. Concurrently, we plan to integrate our data into simulation platforms (e.g., Habitat [34]) to facilitate the development of Sim-to-Real autonomous driving models. These research efforts aim to develop stable, in-the-wild autonomous systems and create comprehensive 3D Digital Twins for precision agriculture.

## 7. Acknowledgment

This work was supported in part by the US Department of Agriculture (grant numbers 2024-67021-42528 and 2022-67022-37021), the Culture, Sports, and Tourism R&D Program through the Korea Creative Content Agency grant funded by the Ministry of Culture, Sports and Tourism in 2024 (International Collaborative Research and Global Talent Development for the Development of Copyright Management and Protection Technologies for Generative AI, RS-2024-00345025), and the Institute of Information & Communications Technology Planning & Evaluation (IITP) grant funded by the Korea government (MSIT) (No. RS-2019-II190079, Artificial Intelligence Graduate School Program, Korea University).

#### References

- Jonathan T. Barron, Ben Mildenhall, Dor Verbin, Pratul P. Srinivasan, and Peter Hedman. Zip-nerf: Anti-aliased grid-based neural radiance fields. *ICCV*, 2023. 3, 5, 7
- [2] Gyusam Chang, Tuan-Anh Vu, Vivek Alumootil, Harris Song, Deanna Pham, Sangpil Kim, and M Khalid Jawed. Reconstruction using the invisible: Intuition from nir and metadata for enhanced 3d gaussian splatting. *arXiv preprint aeXiv:2508.14443*, 2025. 2, 3
- [3] Danpeng Chen, Hai Li, Weicai Ye, Yifan Wang, Weijian Xie, Shangjin Zhai, Nan Wang, Haomin Liu, Hujun Bao, and Guofeng Zhang. PGSR: Planar-Based Gaussian Splatting for Efficient and High-Fidelity Surface Reconstruction. IEEE Transactions on Visualization & Computer Graphics, 31(09):6100–6111, 2025. 4, 7, 16
- [4] Jose Cuaran, Andres Eduardo Baquero Velasquez, Mateus Valverde Gasparino, Naveen Kumar Uppalapati, Arun Narenthiran Sivakumar, Justin Wasserman, Muhammad Huzaifa, Sarita Adve, and Girish Chowdhary. Under-canopy dataset for advancing simultaneous localization and mapping in agricultural robotics. *The International Journal of Robotics Research*, 43(6):739–749, 2023. 2, 3
- [5] Rajitha de Silva, Grzegorz Cielniak, Gang Wang, and Junfeng Gao. Deep learning-based crop row following for infield navigation of agri-robots. *Journal of Field Robotics*, 2023. 2, 3
- [6] Juan Pablo Espejel Flores, Abdurrahman Yilmaz, Luis Arturo Soriano Avendaño, and Grzegorz Cielniak. Comparative analysis of unity and gazebo simulators for digital twins of robotic tomato harvesting scenarios. In Annual Conference Towards Autonomous Robotic Systems, pages 15–27. Springer, 2024. 1
- [7] Nicolai Häni, Pravakar Roy, and Volkan Isler. Minneapple: a benchmark dataset for apple detection and segmentation. IEEE Robotics and Automation Letters, 5(2):852–858, 2020. 2, 3
- [8] Nico Heider, Lorenz Gunreben, Sebastian Zürner, and Martin Schieck. A survey of datasets for computer vision in agriculture. arXiv preprint arXiv:2502.16950, 2025.
- [9] Bernhard Kerbl, Georgios Kopanas, Thomas Leimkühler, and George Drettakis. 3d gaussian splatting for real-time

- radiance field rendering. *ACM Trans. Graph.*, 42(4):139–1, 2023. 4, 7, 8, 5, 11
- [10] Bernhard Kerbl, Andreas Meuleman, Georgios Kopanas, Michael Wimmer, Alexandre Lanvin, and George Drettakis. A hierarchical 3d gaussian representation for real-time rendering of very large datasets. ACM Transactions on Graphics, 43(4), 2024. 4, 7, 8, 9
- [11] Shakiba Kheradmand, Daniel Rebain, Gopal Sharma, Weiwei Sun, Yang-Che Tseng, Hossam Isack, Abhishek Kar, Andrea Tagliasacchi, and Kwang Moo Yi. 3d gaussian splatting as markov chain monte carlo. Advances in Neural Information Processing Systems, 37:80965–80986, 2024. 4, 7, 17
- [12] Jana Kierdorf, Laura Verena Junker-Frohn, Mike Delaney, Mariele Donoso Olave, Andreas Burkart, Hannah Jaenicke, Onno Muller, Uwe Rascher, and Ribana Roscher. Growliflower: An image time-series dataset for growth analysis of cauliflower. *Journal of Field Robotics*, 40(2):173–192, 2023. 3
- [13] Kitae Kim, Aarya Deb, and David J Cappelleri. P-agnav: Range view-based autonomous navigation system for cornfields. *IEEE Robotics and Automation Letters*, 2025. 1
- [14] Jonas Kulhanek and Torsten Sattler. Tetra-NeRF: Representing neural radiance fields using tetrahedra. In *Proceedings of the IEEE/CVF International Conference on Computer Vision*, pages 18458–18469, 2023. 3, 5, 15
- [15] Jonas Kulhanek and Torsten Sattler. NerfBaselines: Consistent and reproducible evaluation of novel view synthesis methods. In *Proceedings of the 39th International Conference on Neural Information Processing Systems (NeurIPS 2025)*, 2025. 7, 5
- [16] Jonas Kulhanek, Songyou Peng, Zuzana Kukelova, Marc Pollefeys, and Torsten Sattler. WildGaussians: 3D gaussian splatting in the wild. In *Proceedings of the 38th Interna*tional Conference on Neural Information Processing Systems, 2024. 4, 7, 22
- [17] Deborah Levy, Amit Peleg, Naama Pearl, Dan Rosenbaum, Derya Akkaynak, Simon Korman, and Tali Treibitz. Seathrunerf: Neural radiance fields in scattering media. In *Proceed*ings of the IEEE/CVF Conference on Computer Vision and Pattern Recognition, pages 56–65, 2023. 5, 21
- [18] Thomas Lowe, Peyman Moghadam, Everard Edwards, Jason Williams, Stephen Brosnan, David Haddon, and Ross Dungavell. Agscan3d viticulture datasets. v1. CSIRO. Data Collection, 2021. 2
- [19] Tao Lu, Mulin Yu, Linning Xu, Yuanbo Xiangli, Limin Wang, Dahua Lin, and Bo Dai. Scaffold-gs: Structured 3d gaussians for view-adaptive rendering. In Proceedings of the IEEE/CVF Conference on Computer Vision and Pattern Recognition, pages 20654–20664, 2024. 4, 7, 14
- [20] Siavash Mahmoudi, Amirreza Davar, Pouya Sohrabipour, Ramesh Bahadur Bist, Yang Tao, and Dongyi Wang. Leveraging imitation learning in agricultural robotics: a comprehensive survey and comparative analysis. Frontiers in Robotics and AI, 11:1441312, 2024. 1
- [21] Muneeb Elahi Malik and Md Sultan Mahmud. A digital twin-enabled approach for precision weed management in

- specialty crops using a 4-dof robotic system. In 2024 ASABE Annual International Meeting, page 1. American Society of Agricultural and Biological Engineers, 2024. 1
- [22] Saswat Subhajyoti Mallick, Rahul Goel, Bernhard Kerbl, Markus Steinberger, Francisco Vicente Carrasco, and Fernando De La Torre. Taming 3dgs: High-quality radiance fields with limited resources. In SIGGRAPH Asia 2024 Conference Papers, New York, NY, USA, 2024. Association for Computing Machinery. 4, 7, 8, 10
- [23] Elias Marks, Jonas Bömer, Federico Magistri, Anurag Sag, Jens Behley, and Cyrill Stachniss. Bonnbeetclouds3d: A dataset towards point cloud-based organ-level phenotyping of sugar beet plants under real field conditions. In 2024 IEEE/RSJ International Conference on Intelligent Robots and Systems (IROS), pages 1804–1811. IEEE, 2024. 2, 3
- [24] Nicolas Moenne-Loccoz, Ashkan Mirzaei, Or Perel, Riccardo de Lutio, Janick Martinez Esturo, Gavriel State, Sanja Fidler, Nicholas Sharp, and Zan Gojcic. 3d gaussian ray tracing: Fast tracing of particle scenes. ACM Transactions on Graphics and SIGGRAPH Asia, 2024. 4, 7, 8, 12
- [25] Abhishake Reddy Onteddu, RamMohan Reddy Kundavaram, Arjun Kamisetty, Jaya Chandra Srikanth Gummadi, and Aditya Manikyala. Enhancing agricultural efficiency with robotics and ai-powered autonomous farming systems. *Malaysian Journal of Medical and Biological Re*search, 12(1):7–22, 2025. 1
- [26] Shivam K Panda, Yongkyu Lee, and M Khalid Jawed. Agronav: Autonomous navigation framework for agricultural robots and vehicles using semantic segmentation and semantic line detection. In Proceedings of the IEEE/CVF Conference on Computer Vision and Pattern Recognition, pages 6272–6281, 2023. 2, 3
- [27] Piyushkumar Patel and Rakeshkumar Patel. Ai-driven agricultural robotics: Integrating gnns and llms for comprehensive field-based crop health prediction and management. Available at SSRN 5355686, 2025. 1
- [28] Hongxing Peng, Shangkun Guo, Xiangjun Zou, Hongjun Wang, Juntao Xiong, and Qijun Liang. Uavo-nerf: 3d reconstruction of orchards and semantic segmentation of fruit trees based on neural radiance field in uav images. *Computers and Electronics in Agriculture*, 237:110631, 2025. 1
- [29] Taihú Pire, Martín Mujica, Javier Civera, and Ernesto Kofman. The rosario dataset: Multisensor data for localization and mapping in agricultural environments. *The International Journal of Robotics Research*, 38(6):633–641, 2019. 2
- [30] Kerui Ren, Lihan Jiang, Tao Lu, Mulin Yu, Linning Xu, Zhangkai Ni, and Bo Dai. Octree-gs: Towards consistent real-time rendering with lod-structured 3d gaussians. *arXiv* preprint arXiv:2403.17898, 2024. 4, 7, 8
- [31] Weining Ren, Zihan Zhu, Boyang Sun, Jiaqi Chen, Marc Pollefeys, and Songyou Peng. Nerf on-the-go: Exploiting uncertainty for distractor-free nerfs in the wild. In *IEEE/CVF Conference on Computer Vision and Pattern Recognition* (CVPR), 2024. 3
- [32] Johannes Lutz Schönberger and Jan-Michael Frahm. Structure-from-Motion Revisited. In *Conference on Computer Vision and Pattern Recognition (CVPR)*, 2016. 7, 4

- [33] A Subeesh and Naveen Chauhan. Agricultural digital twin for smart farming: A review. Green Technologies and Sustainability, page 100299, 2025. 1
- [34] Andrew Szot, Alex Clegg, Eric Undersander, Erik Wijmans, Yili Zhao, John Turner, Noah Maestre, Mustafa Mukadam, Devendra Chaplot, Oleksandr Maksymets, Aaron Gokaslan, Vladimir Vondrus, Sameer Dharur, Franziska Meier, Wojciech Galuba, Angel Chang, Zsolt Kira, Vladlen Koltun, Jitendra Malik, Manolis Savva, and Dhruv Batra. Habitat 2.0: Training home assistants to rearrange their habitat. In Advances in Neural Information Processing Systems (NeurIPS), 2021. 8
- [35] Matthew Tancik, Ethan Weber, Evonne Ng, Ruilong Li, Brent Yi, Justin Kerr, Terrance Wang, Alexander Kristoffersen, Jake Austin, Kamyar Salahi, Abhik Ahuja, David McAllister, and Angjoo Kanazawa. Nerfstudio: A modular framework for neural radiance field development. In ACM SIGGRAPH 2023 Conference Proceedings, 2023. 3, 5, 20
- [36] Jianyuan Wang, Minghao Chen, Nikita Karaev, Andrea Vedaldi, Christian Rupprecht, and David Novotny. Vggt: Visual geometry grounded transformer. In Proceedings of the IEEE/CVF Conference on Computer Vision and Pattern Recognition, 2025. 7, 4
- [37] Qi Wu, Janick Martinez Esturo, Ashkan Mirzaei, Nicolas Moenne-Loccoz, and Zan Gojcic. 3dgut: Enabling distorted cameras and secondary rays in gaussian splatting. Conference on Computer Vision and Pattern Recognition (CVPR), 2025. 4, 7, 18
- [38] Vickie Ye, Ruilong Li, Justin Kerr, Matias Turkulainen, Brent Yi, Zhuoyang Pan, Otto Seiskari, Jianbo Ye, Jeffrey Hu, Matthew Tancik, and Angjoo Kanazawa. gsplat: An open-source library for gaussian splatting. *Journal of Machine Learning Research*, 26(34):1–17, 2025. 4, 7, 8, 13
- [39] Ariyan Zarei, Bosheng Li, James C Schnable, Eric Lyons, Duke Pauli, Kobus Barnard, and Bedrich Benes. Plantsegnet: 3d point cloud instance segmentation of nearby plant organs with identical semantics. *Computers and Electronics in Agriculture*, 221:108922, 2024. 2
- [40] Dongbin Zhang, Chuming Wang, Weitao Wang, Peihao Li, Minghan Qin, and Haoqian Wang. Gaussian in the wild: 3d gaussian splatting for unconstrained image collections. In European Conference on Computer Vision, pages 341–359. Springer, 2024. 4, 7, 19
- [41] Jianzhong Zhu, Ruifang Zhai, He Ren, Kai Xie, Aobo Du, Xinwei He, Chenxi Cui, Yinghua Wang, Junli Ye, Jiashi Wang, et al. Crops3d: a diverse 3d crop dataset for realistic perception and segmentation toward agricultural applications. *Scientific Data*, 11(1):1438, 2024. 2, 3

## AgriChrono: A Multi-modal Dataset Capturing Crop Growth and Lighting Variability with a Field Robot

## Supplementary Material

## **Contents**

AgriChrono Platform
A.1. Software Stack
AgriChrono Dataset
B.1. Collection Schedule
B.2. Robot Trajectory
AgriChrono Benchmark
C.1. Extrinsic Camera Pose
C.2. NeRF-based Method
C.3. Qualitative Results

## A. AgriChrono Platform

## A.1. Software Stack

The AgriChrono platform is deployed on a NVIDIA Jetson AGX Orin 64GB Developer Kit (Jetson) running JetPack 6.2 (L4T 36.4.3). This embedded system utilizes ROS2 Humble for robot control and a gs\_usb kernel module, externally recompiled for the L4T 36.4.3 kernel, to enable the CAN bus interface. The sensing suite includes ZED SDK v5.0.2 with the ZED Link Duo v1.3.0 driver for stereo vision and Livox SDK2 for LiDAR. Additionally, Tailscale VPN is used for robust headless connectivity and static IP assignment. The system architecture comprises six core modules, as illustrated in Fig. 8.

The 1-janus-streaming module manages all remote operations, including real-time video streaming, associated camera PTZ control, robot teleoperation, and data recording. This module offers a low-latency teleoperation interface by utilizing a Janus WebRTC server in conjunction with a GStreamer pipeline. The GStreamer pipeline leverages the Jetson's onboard nvv412h264enc hardware encoder to stream a 640 x 360 @ 15 FPS video at a low bitrate (300 kbps) via RTP. This hardware-accelerated, low-bitrate configuration is critical for enabling real-time teleoperation over long-distance connections. A custom Flask-SocketIO Web UI provides the operator interface, rendering the streaming video while providing simultaneous controls for camera PTZ, robot teleoperation, system monitoring, and data recording. Furthermore, a fail-safe mechanism is integrated, issuing a zero-velocity command upon browser disconnection or loss of focus to prevent erratic robot behavior. The Web UI is shown in Fig. 2 of the main paper.

Robot control is managed by the **2\_scout-ros2-control** module. This module is based on the AgileX scout\_ros2 stack and includes a patch file to ensure compatibility with ROS2 Humble, along with an installation script for the gs\_usb kernel module, which enables CAN bus communication on the Jetson. This module receives geometry\_msgs.msg::Twist messages from the Web UI's Flask backend to drive the robot. The operator can set the values for linear velocity (ranging from 0.1 m/s to 1.5 m/s) and angular velocity (from 0.1 to 1.0 rad/s) via the Web UI, ensuring consistent and uniform data collection.

Two dedicated modules handle multi-modal data logging. The 3\_zed-data-tools module captures synchronized dual ZED X streams (HD1080 @ 15 FPS, NEURAL Depth) and IMU data, saving them as .svo2 and .csv files. Concurrently, the 4\_livox-data-tools module uses a custom recorder\_sync.cpp built on Livox SDK2 to log synchronized LiDAR point clouds (pointcloud\_sync.bin) and IMU data (imu\_sync.bin). To ensure precise temporal alignment between these independent sensors, a central software-trigger mechanism was implemented. When the operator starts a recording, the central Flask server immediately generates a high-precision UNIX timestamp (time.time()) and writes it to a central sync\_time.txt file. This file serves as the master time zero for the entire recording session. The ZED (data\_svo\_sync.py) and custom Livox (recorder\_sync.cpp) recording processes are then launched simultaneously as subprocesses. Both of these custom recorders are designed to read this shared sync\_time.txt timestamp, using it as their temporal origin, ensuring all data streams are precisely aligned to a single, software-defined start time.

Finally, two service modules ensure robust field deployment. The 5\_systemd module automates data management. It contains scripts that use udev rules to trigger an automatic data backup the moment an external HDD is connected, as well as a systemd service that maintains an rclone mount for automatic uploads to a Box cloud server. The 6\_network module provides headless connectivity. It runs a boot-time service that emails the Jetson's IP address, Wi-Fi SSID, and Link speed to the operator. This enables users to remotely monitor and access the system without requiring direct terminal interaction.

This entire integrated system ran stably for one month in real-world field conditions, demonstrating that it enables convenient operation and data collection even for users without expert knowledge of Ubuntu or terminal commands.

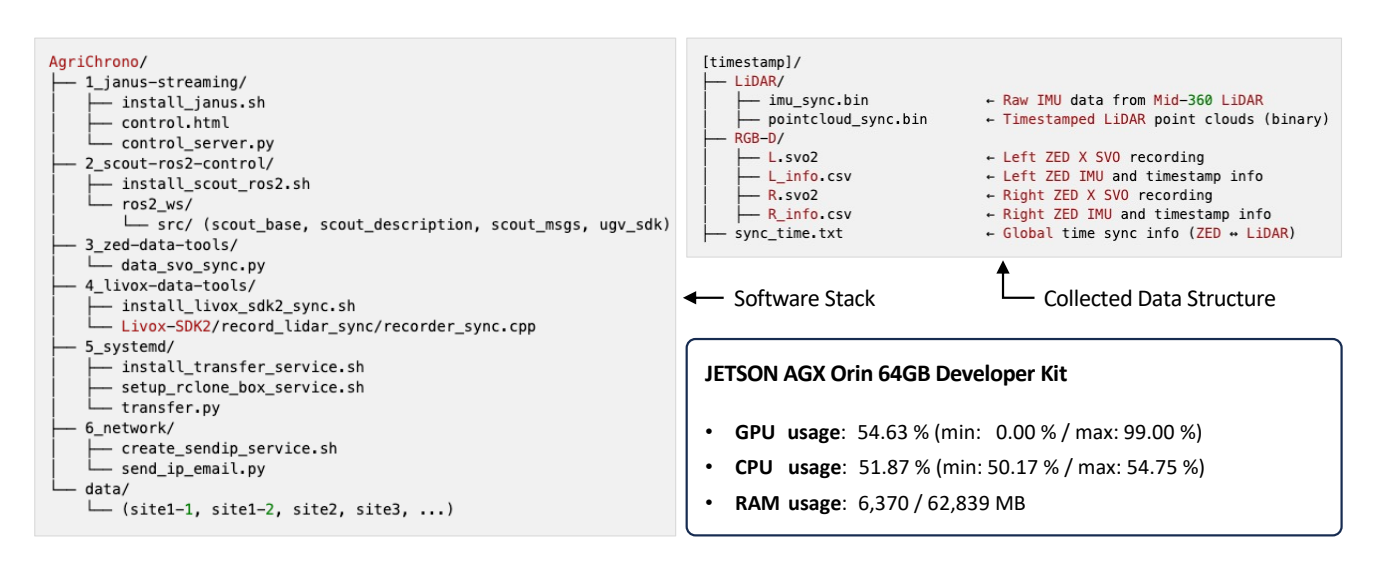


Figure 8. AgriChrono Platform Software and Data Logging Architecture. Left, the complete software stack architecture deployed on the NVIDIA Jetson AGX Orin, detailing the six core modules. Top right, the data structure for a single recording session, showing the software-triggered, time-synchronized outputs from the ZED cameras (.svo2) and Livox LiDAR (.bin). Bottom right, system resource (CPU, GPU, RAM) usage during a typical data logging operation.

## **B.** AgriChrono Dataset

#### **B.1. Collection Schedule**

The calendar on the right visually details the data collection schedule for the *AgriChrono* dataset, which is introduced in Sec. 3.1 of the main paper. As outlined, the collection was structured into two primary phases based on crop growth.

Phase 1 (July 2–21), corresponding to the active growth period, involved intensive sampling at the Main Canola Site (Site 1). To capture diverse illumination and rapid morphological changes, data were collected four times daily at 06:00 (sunrise), 11:00 (high sun), 16:00 (afternoon), and 21:00 (sunset). Each of sessions included two complete clockwise and counterclockwise traversals of this site.

**Phase 2 (July 22–August 1)** began as crop growth visibly slowed and plateaued. During this period, the collection frequency for Site 1 was reduced to twice per week.

Data collection was subject to environmental constraints, with sessions omitted due to rain or excessively muddy ground. Consequently, certain Phase 1 days exhibit fewer than the targeted four sessions. Concurrently, to ensure data diversity, auxiliary Sites 2 and 3 were sampled selectively (1-2 times/week) only when significant visual changes were observed.

The comprehensive statistics for the entire multi-modal dataset gathered from this rigorous, month-long schedule are summarized in Table 2 of the main paper.

Table 5. **AgriChrono Dataset Collection Schedule.** This calendar visualizes the collection schedule, detailing the frequency for Phase 1 (July 2–21) and Phase 2 (July 22–Aug 1).

Sun	Mon	Tue	Wed	Thu	Fri	Sat
		7/1	2	3	4	5
			S1 (4) S2 (1) S3 (1)	S1 (3) S3 (1)	S1 (3)	S1 (2)
6	7	8	9	10	11	12
				S1 (3)		
S1 (4)	S1 (4)	S1 (4)	S1 (4)	S2 (1)	S1 (4)	S1 (4)
				S3 (1)		
13	14	15	16	17	18	19
S1 (4)				S1 (4)		
S2 (1)	S1 (4)	S1 (4)	S1 (4)	S2 (1)	S1 (4)	S1 (4)
S3 (1)				S3 (1)		
20	21	22	23	24	25	26
	S1 (2)					
S1 (4)	S2 (1)	S1 (1)		S1 (1)		
	S3 (1)					
27	28	29	30	31	8/1	
	S1 (1)				S1 (1)	
	S2 (1)	S1 (1)	S1 (1)	S1 (1)	S2 (1)	
	S3 (1)				S3 (1)	

## **B.2. Robot Trajectory**

To generate robust robot trajectories, we fused the Visual-Inertial Odometry (VIO) outputs from two ZED X cameras via averaging. This method yielded stable trajectories for Site 1 and Site 3, which benefited from shorter travel distances and correspondingly stable FPS (as detailed in Table 2 of the main paper). However, as noted in Section 6 (Limitations) of our main paper, Site 2 exhibited progressively inaccurate trajectories on longer runs, which we attribute to increasing computational and thermal load on the embodied device. We aim to address this hardware-level bottleneck in future work by refining the platform structure to mitigate thermal issues and developing software for dynamic time-synchronization.

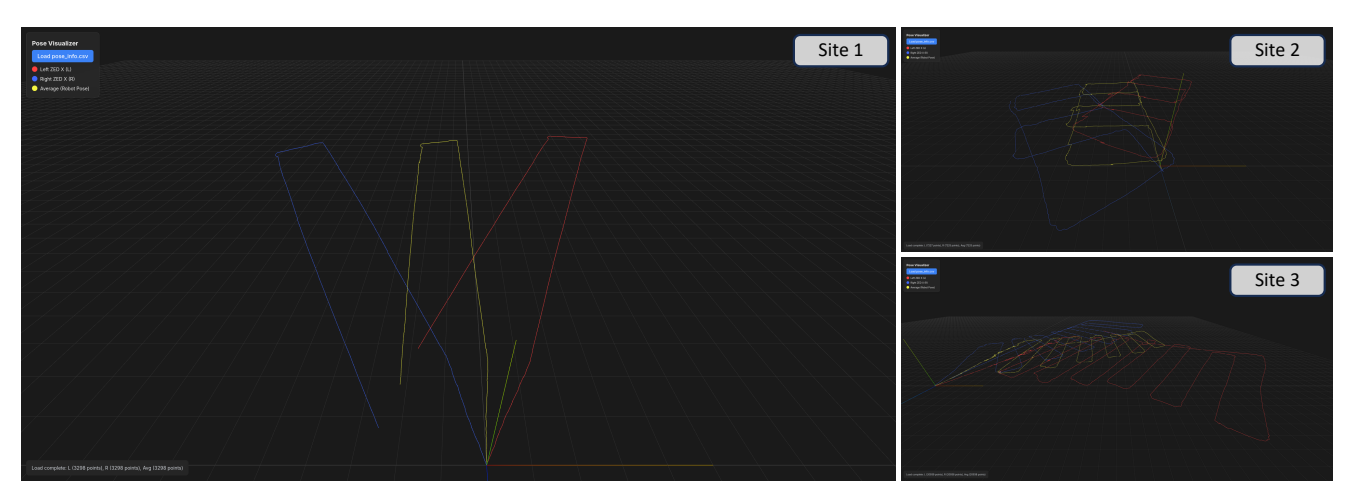


Figure 9. **Visualization of trajectories for Sites 1, 2, and 3.** The *AgriChrono* Platform's trajectory (yellow line) is derived by averaging the VIO outputs from the Left ZED X Camera (red line) and the Right ZED X Camera (blue line). As depicted in Fig. 2 of the main paper, the shape of the trajectory accurately reflects the field's actual structure.

## C. AgriChrono Benchmark

#### C.1. Extrinsic Camera Pose

To quantitatively assess pose reliability, we evaluate the inter-frame trajectory smoothness by computing the Mean, Standard Deviation (Std. Dev.), and Coefficient of Variation (CV) of the distance between adjacent poses (sampled every 7 frames). Given that our UGV acquired the data at a constant velocity (0.2 m/s, avg. 14.7 FPS, shown in Table 2 of the main paper), *AgriChrono* benchmark datasets should theoretically yield a uniform inter-frame distance of ~9 cm. As demonstrated in Table 6, the poses from our dataset (derived from the robotic platform's RGB and IMU sensors) adhere closely to this, achieving a consistent mean distance near 9 cm and a very low CV. This confirms their high reliability and smoothness.

To demonstrate the superiority of our robotic dataset, we benchmarked pose extraction performance against the state-of-the-art learning-based VGGT [36] and traditional COLMAP [32]. For VGGT, the unitless nature of the output precludes direct metric validation, while its high CV exposes significant, unrealistic inter-frame variability. Furthermore, SfM pipelines utilizing COLMAP failed completely to resolve poses in these dynamic, non-rigid scenes. This confirms that our robotic, multimodal collection strategy for non-rigid, in-the-wild environments yields reliable extrinsic camera poses whose quality is readily verifiable.

Table 6. **Quantitative Pose Analysis.** The *AgriChrono* dataset exhibits high pose reliability, featuring consistent, low-variance inter-frame displacement and physically meaningful scales for direct evaluation.

	Condition	Li	ghting Vari	Growth Span (6 AM)				
	Condition	06:00 AM	11:00 AM	04:00 PM	09:00 PM	Day 6	Day 13	Day 20
ouo	Mean (µ)	0.0920	0.0912	0.0909	0.0915	0.0887	0.0882	0.0912
AgriChrono	Std. Dev. $(s) \downarrow$	0.0131	0.0063	0.0049	0.0061	0.0257	0.0108	0.0074
Ag	$\mathrm{CV}\left(s/\mu\right)\downarrow$	0.1418	0.0688	0.0542	0.0662	0.2892	0.1228	0.0809
[36]	Mean (µ)	0.0416	0.0486	0.0386	0.0281	0.0286	0.0239	0.0249
VGGT	Std. Dev. $(s) \downarrow$	0.0608	0.0887	0.0367	0.0216	0.0079	0.0092	0.0045
Λ	$\mathrm{CV}\left(s/\mu\right)\downarrow$	1.4618	1.8267	0.9520	0.7700	0.2775	0.3825	0.1823

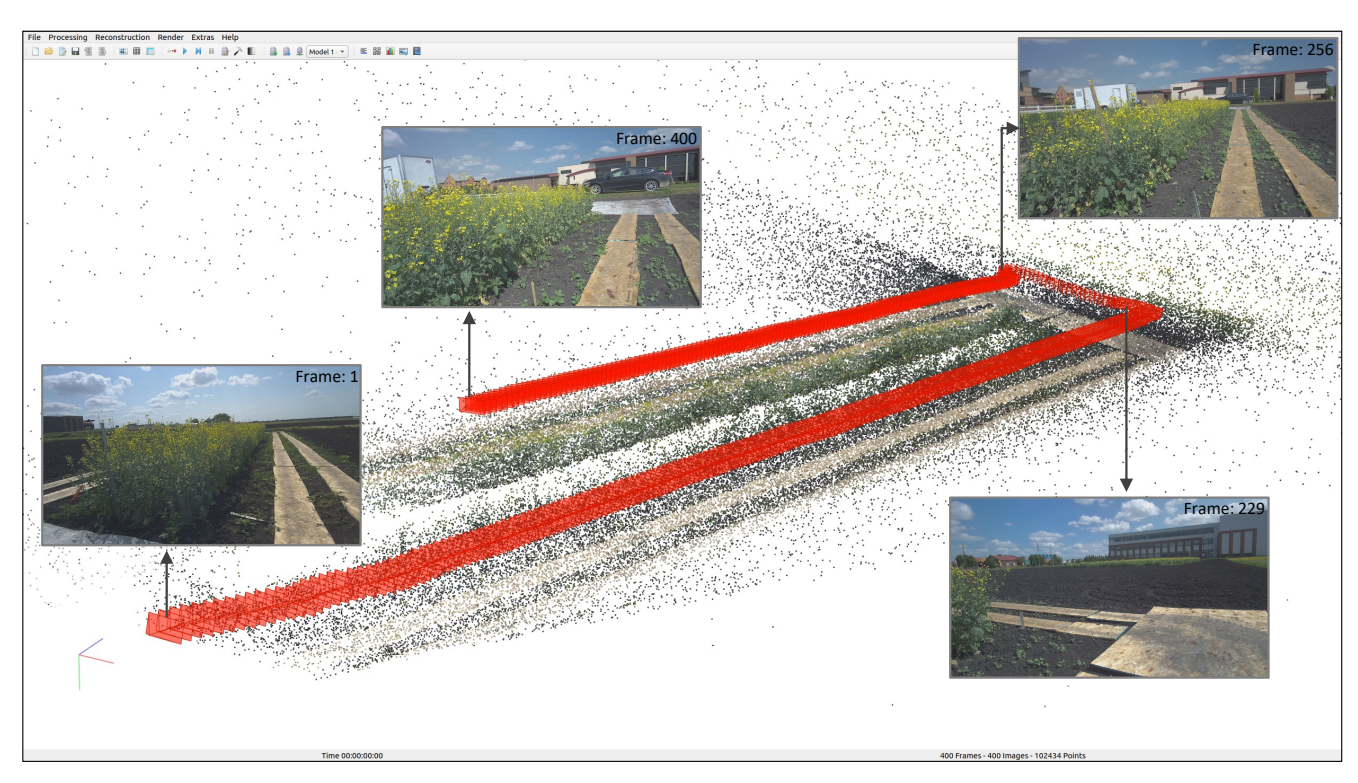


Figure 10. COLMAP Visualization of the AgriChrono Benchmark Dataset. The benchmark data, acquired using a robot moving at a constant velocity, provides reliable camera poses and a robust initial sparse point cloud derived from its synchronized RGB, Depth, and IMU sensors. The COLMAP visualization confirms this, showing 400 camera poses sampled every 7 frames, which are uniformly spaced (approx. 9 cm) along the robot's trajectory. The visualization shown utilizes the 'Lighting Variance 04:00 PM' dataset.

#### C.2. NeRF-based Method

Table 7. **Novel View Synthesis Benchmark** on the *AgriChrono* dataset (Site  $1_{CCW}$ ), specifically evaluating NeRF-based model performance under **Lighting Variance** and **Growth Span**. Consistent with Table 3 of the main paper, four recent state-of-the-art methods were evaluated across a total of seven distinct conditions. Quantitative performance is reported using the PSNR and SSIM metrics.

Condition	Lighting Variance (Day 19)						Growth Span (6 AM)							
Condition	06:00 AM		11:00 AM		04:00 PM		09:00 PM		Day 6		Day 13		Day 20	
Method	PSNR↑	SSIM↑	PSNR↑	SSIM↑	PSNR↑	SSIM↑	PSNR↑	SSIM↑	PSNR↑	SSIM↑	PSNR↑	SSIM↑	PSNR↑	SSIM↑
Zip-NeRF [1]	29.582	0.7953	25.923	0.7562	27.466	0.7663	30.675	0.8065	25.943	0.6097	28.844	0.7742	29.418	0.8105
Tetra-NeRF [14]	28.225	0.7333	24.057	0.6068	25.564	0.6458	29.337	0.7558	25.324	0.5976	27.096	0.6581	27.388	0.7020
NerfStudio [35]	23.703	0.6389	20.275	0.4353	21.573	0.5007	24.739	0.6555	22.133	0.4449	18.809	0.4454	23.194	0.5809
SeaThru-NeRF [17]	25.371	0.6274	21.421	0.4415	22.885	0.4975	26.456	0.6527	22.691	0.4429	21.488	0.4601	24.084	0.5681

In addition to the Gaussian Splatting (GS) methods discussed in Sec. 5 of the main paper, we also benchmarked key NeRF-based approaches. The research trend for NeRF-based methods has noticeably slowed since the introduction of 3D Gaussian Splatting [9] in 2023. This shift is largely attributable to the significant computational overhead inherent to NeRF models, which demand substantial GPU resources and extensive training time, as detailed in Table 8. Despite this trend, when evaluated purely on performance metrics, top-tier NeRF methods like Zip-NeRF [1] still demonstrate exceptionally high

Table 8. **Resource usage of NeRF Baselines.** All methods were evaluated on an NVIDIA RTX 6000 Ada GPU using the NerfBaselines [15] framework.

Year	Method	<b>Training Time</b>	GPU Mem.
	Zip-NeRF [1]	4h 27m 45s	32,448 MB
2023	Tetra-NeRF [14]	17h 53m 4s	13,708 MB
2023	NerfStudio [35]	6m 53s	4,198 MB
2023	SeaThru-NeRF [17]	11h 51m 45s	37,218 MB

scores, as shown in Table 7. This indicates that while the research landscape has pivoted toward GS-based solutions for their efficiency, the rendering quality achieved by leading NeRF models often remains the superior benchmark.

## C.3. Qualitative Results

As an extension of Fig. 7 in the main paper, we present high-resolution Novel View Synthesis results for each scenario, corresponding to the Gaussian Splatting-based benchmark methods from Sec. 5 of the main paper and the NeRF-based methods from Sec. C.2. Fig. 11 provides the Ground Truth image. The results from the benchmarked methods, spanning from Fig. 13 through Fig. 27, are organized in descending order of performance (SSIM) based on the scores in Benchmark Table 3 in the main paper and Table 7. It is clearly observable that the qualitative result quality degrades in correspondence with these quantitative values.



Figure 11. Qualitative Ground Truth Visualization for AgriChrono Benchmark

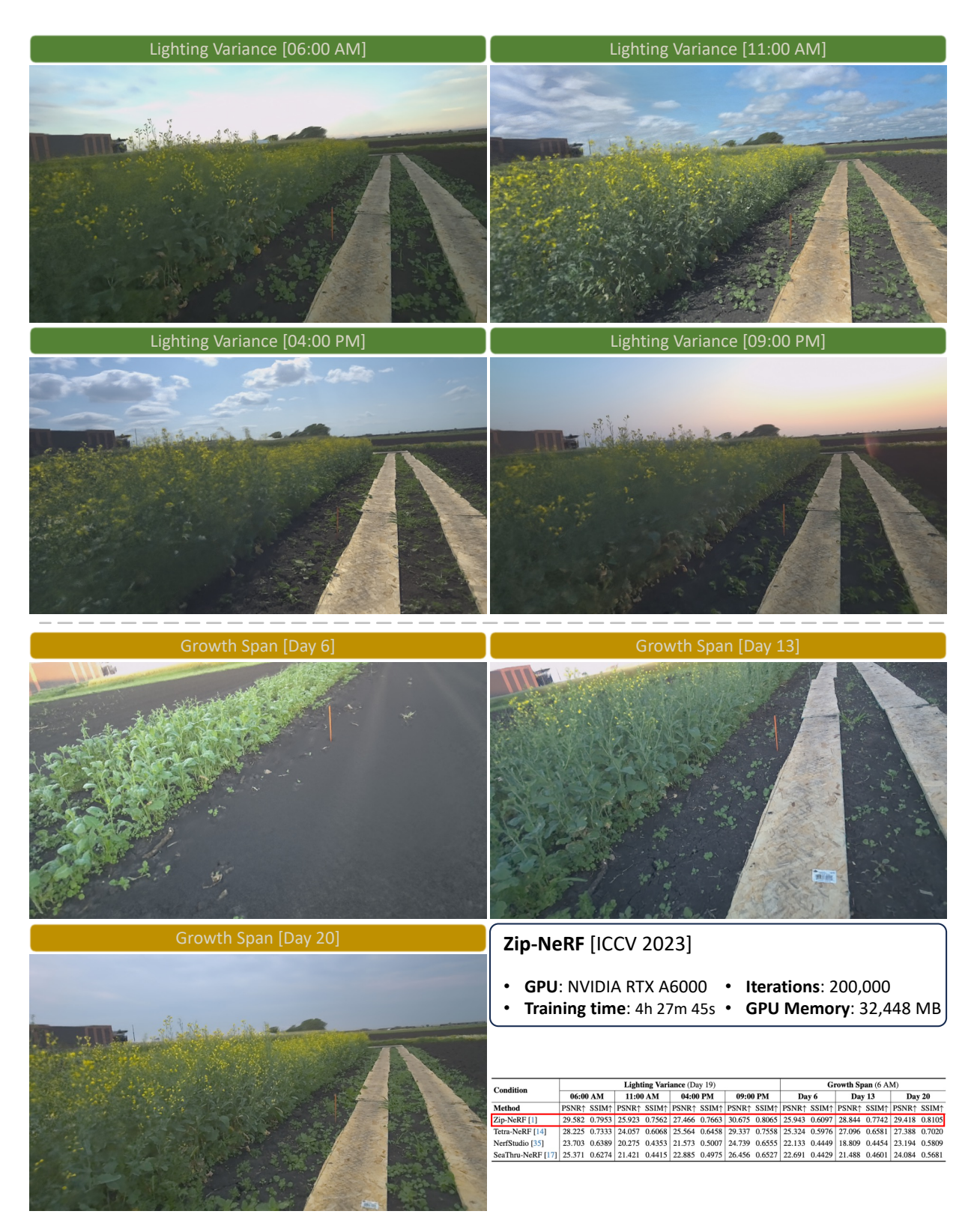


Figure 12. Qualitative Novel View Synthesis Results of Zip-NeRF [1]

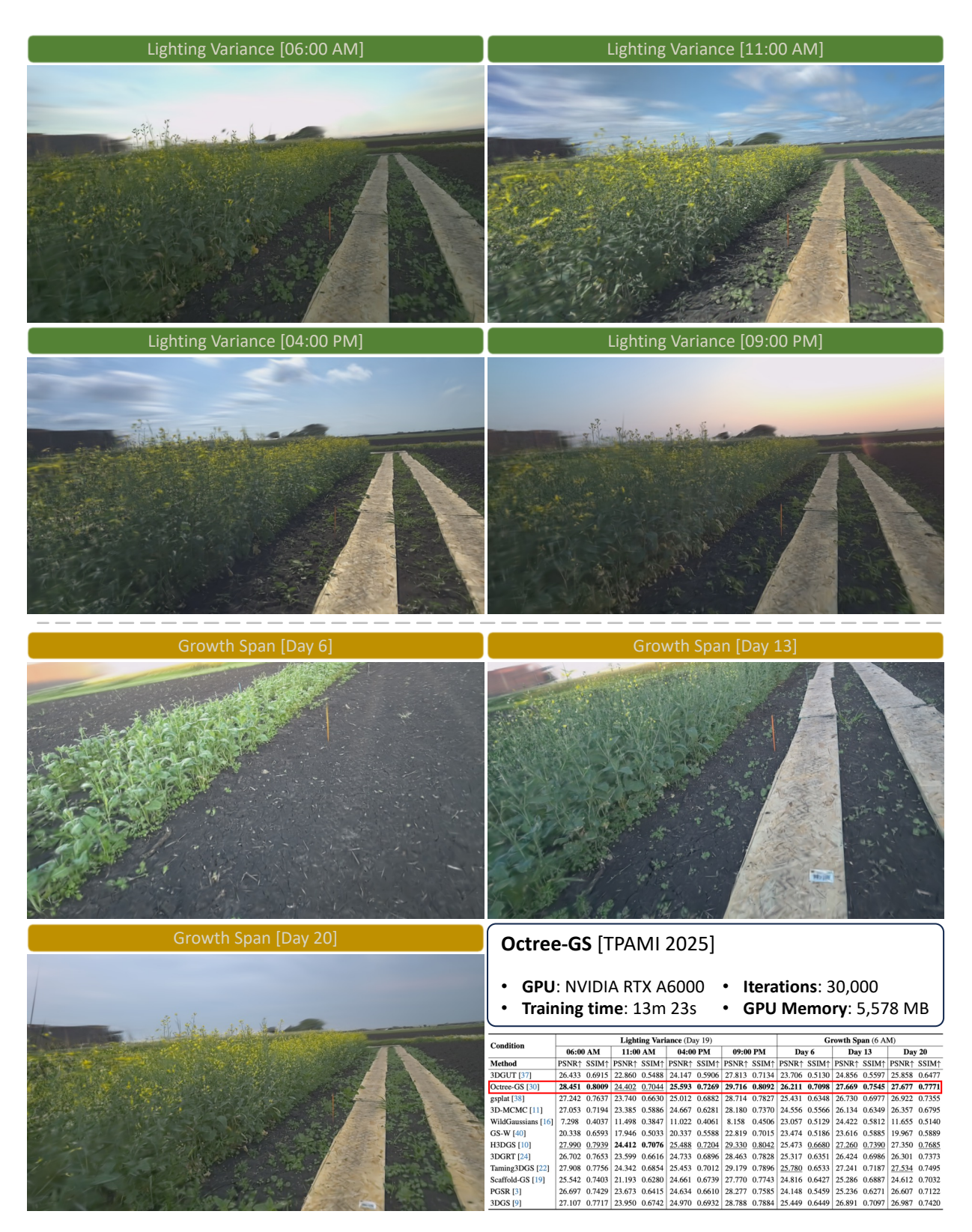


Figure 13. Qualitative Novel View Synthesis Results of Octree-GS [30]



Figure 14. Qualitative Novel View Synthesis Results of Hierarchical-3DGS [10]



Figure 15. Qualitative Novel View Synthesis Results of Taming-3DGS [22]

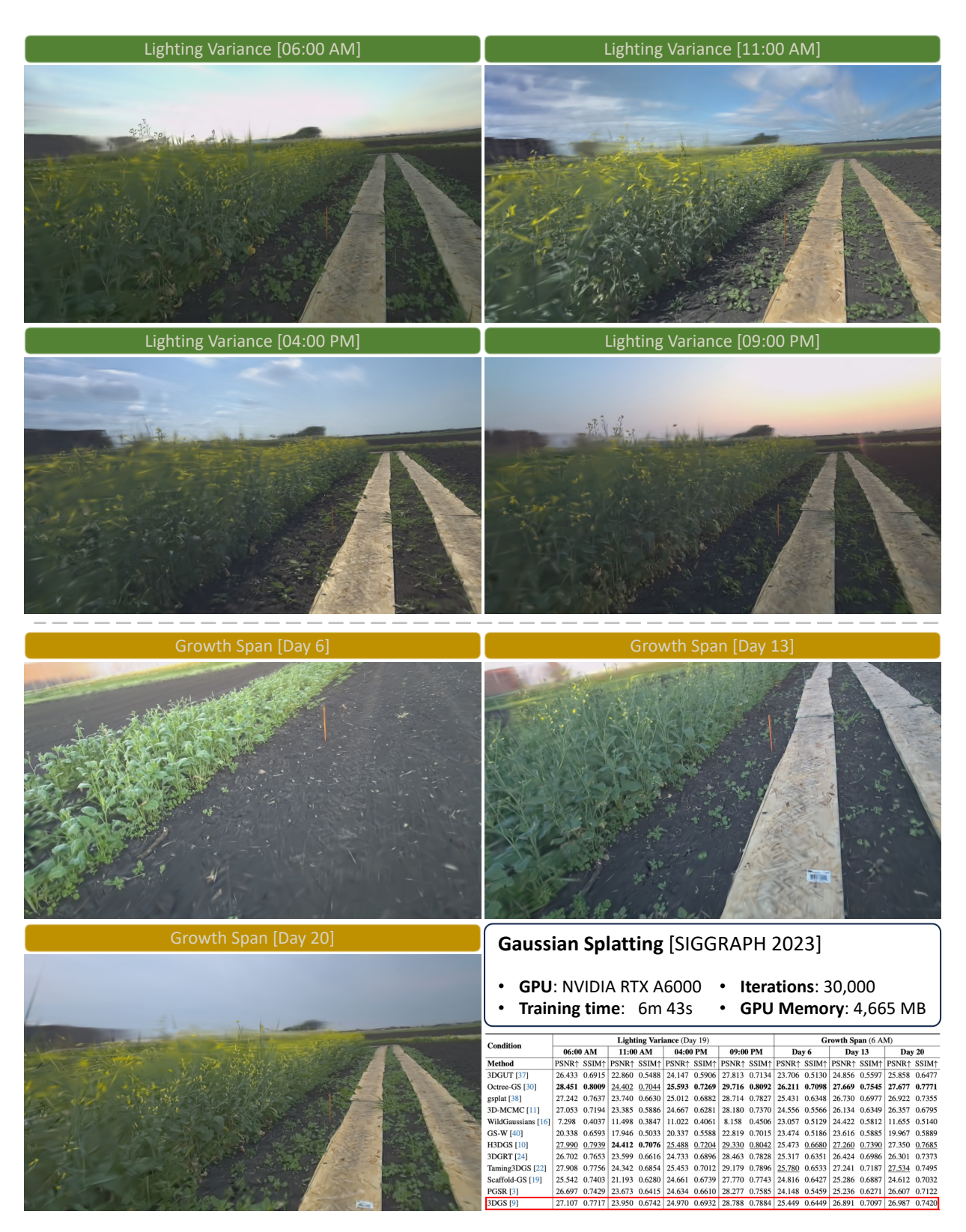


Figure 16. Qualitative Novel View Synthesis Results of Gaussian-Splatting [9]

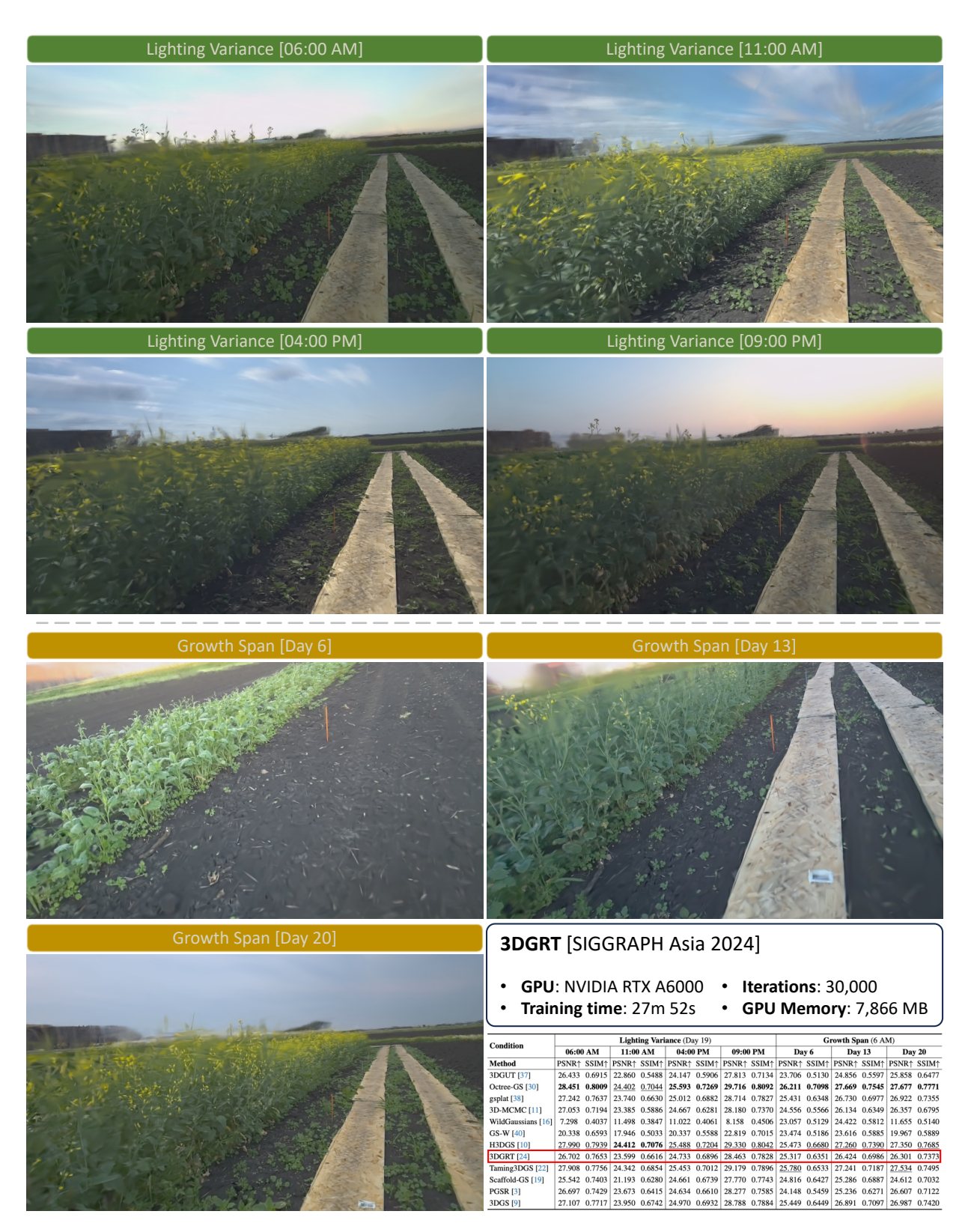


Figure 17. Qualitative Novel View Synthesis Results of 3DGRT [24]

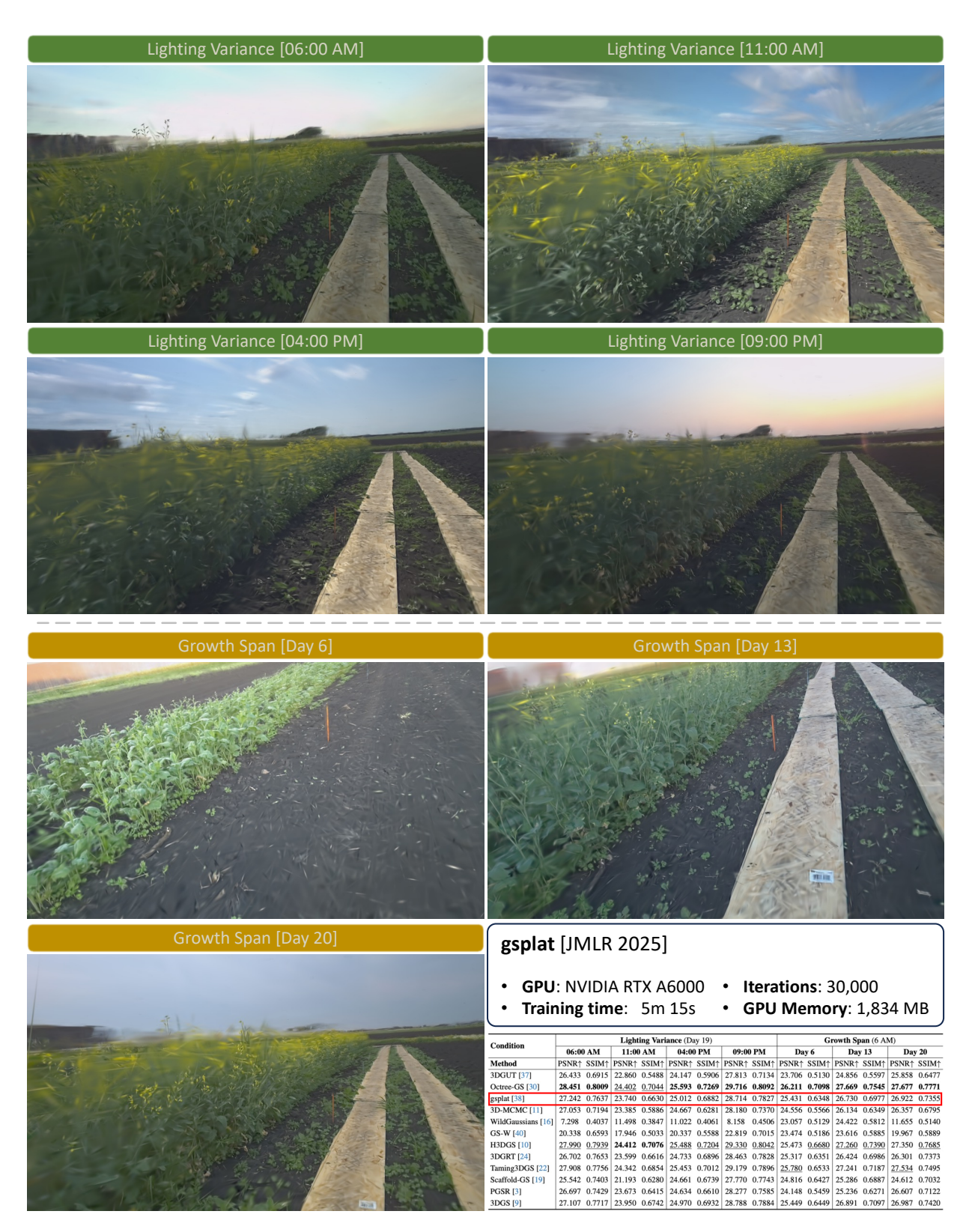


Figure 18. Qualitative Novel View Synthesis Results of gsplat [38]



Figure 19. Qualitative Novel View Synthesis Results of Scaffold-GS [19]

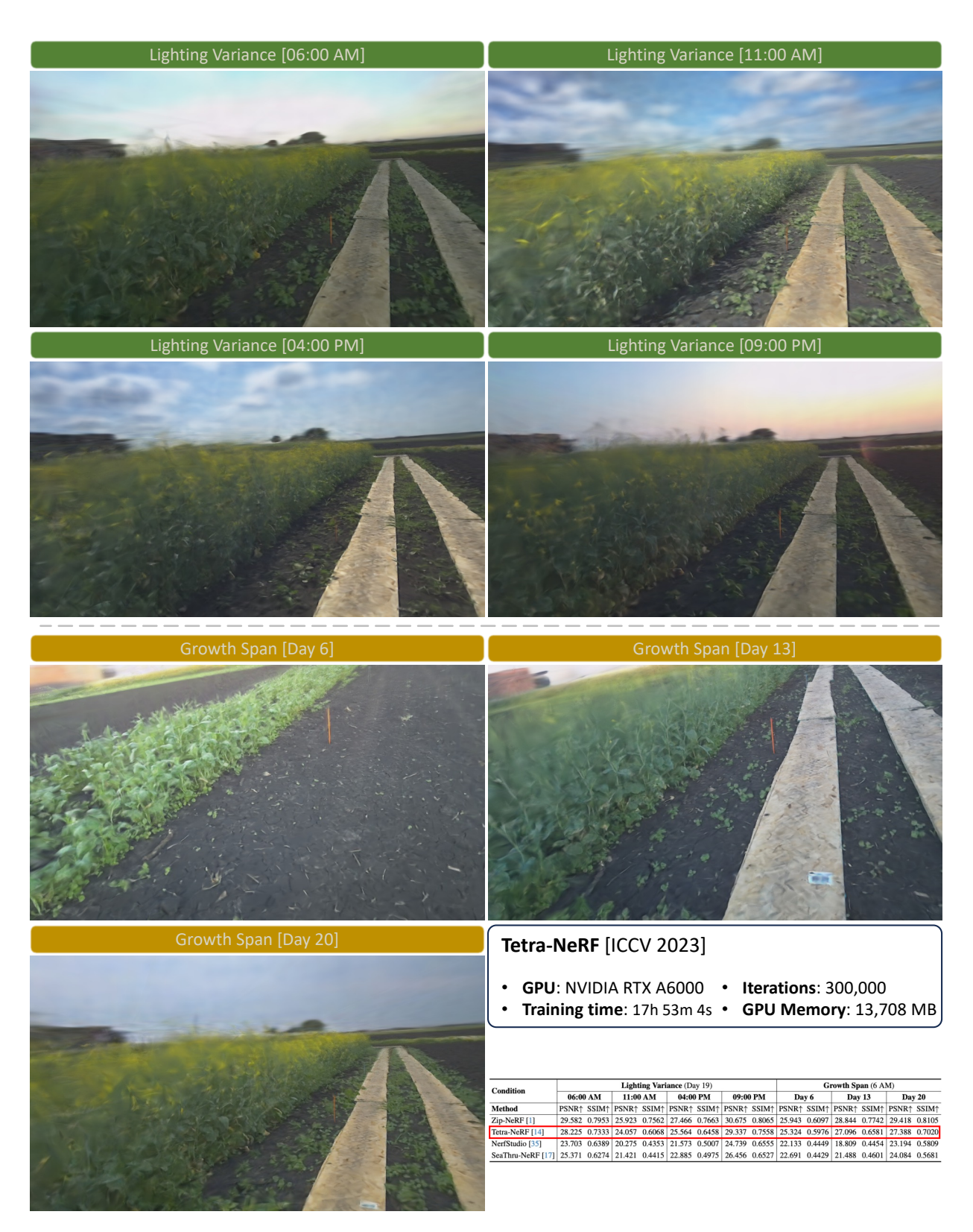


Figure 20. Qualitative Novel View Synthesis Results of Tetra-NeRF [14]

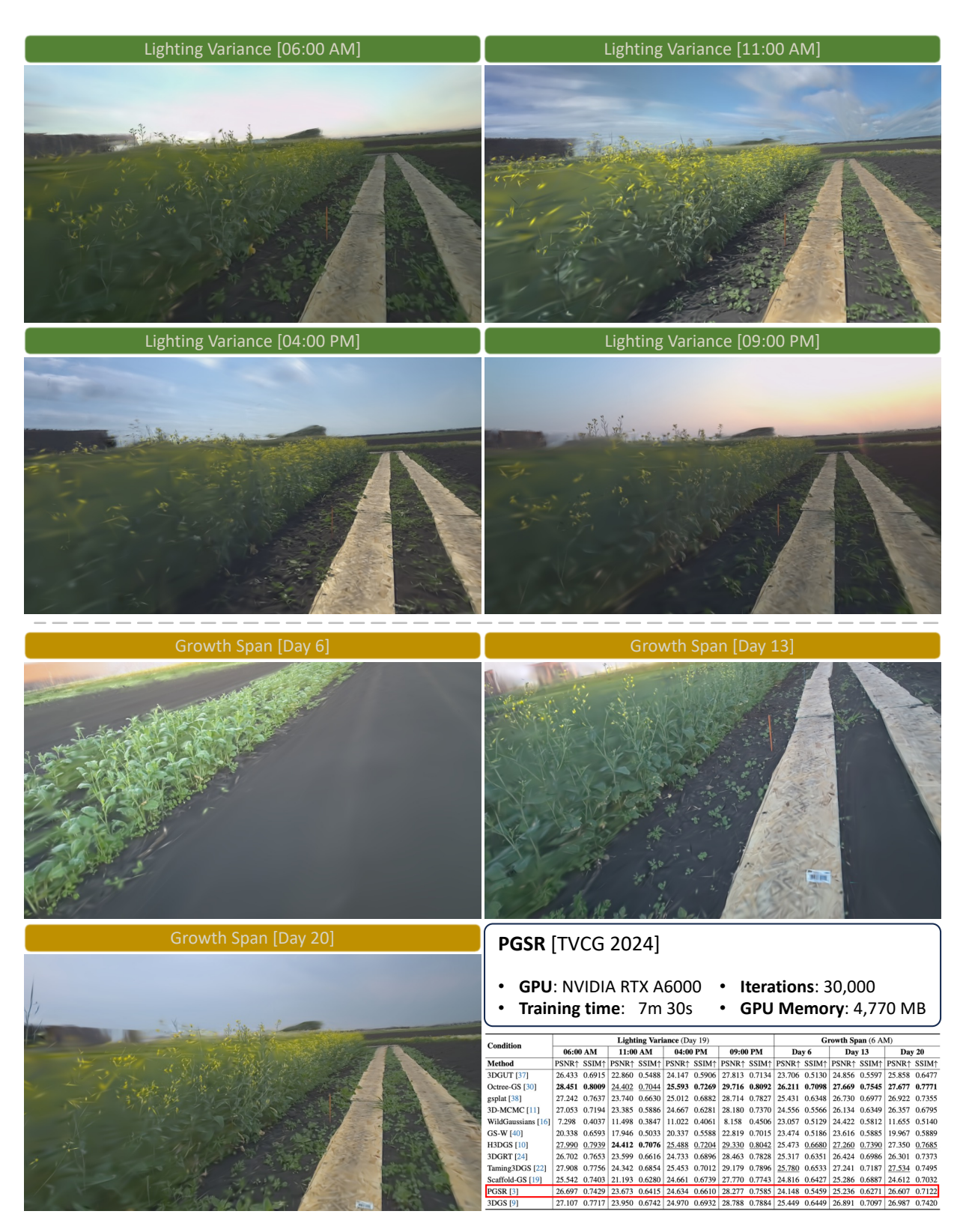


Figure 21. Qualitative Novel View Synthesis Results of PGSR [3]

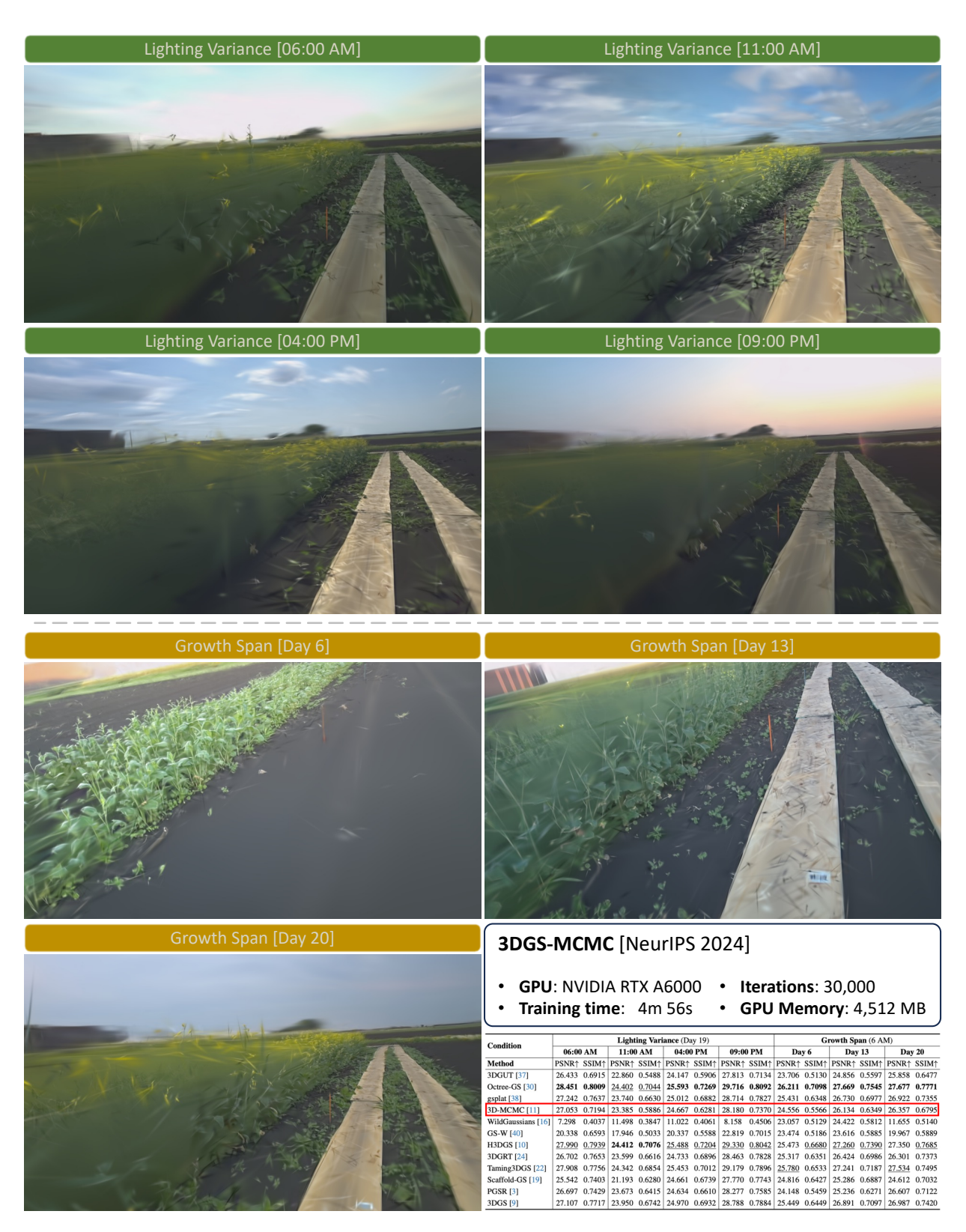


Figure 22. Qualitative Novel View Synthesis Results of 3DGS-MCMC [11]



Figure 23. Qualitative Novel View Synthesis Results of 3DGUT [37]



Figure 24. Qualitative Novel View Synthesis Results of Gaussian-in-the-Wild [40]

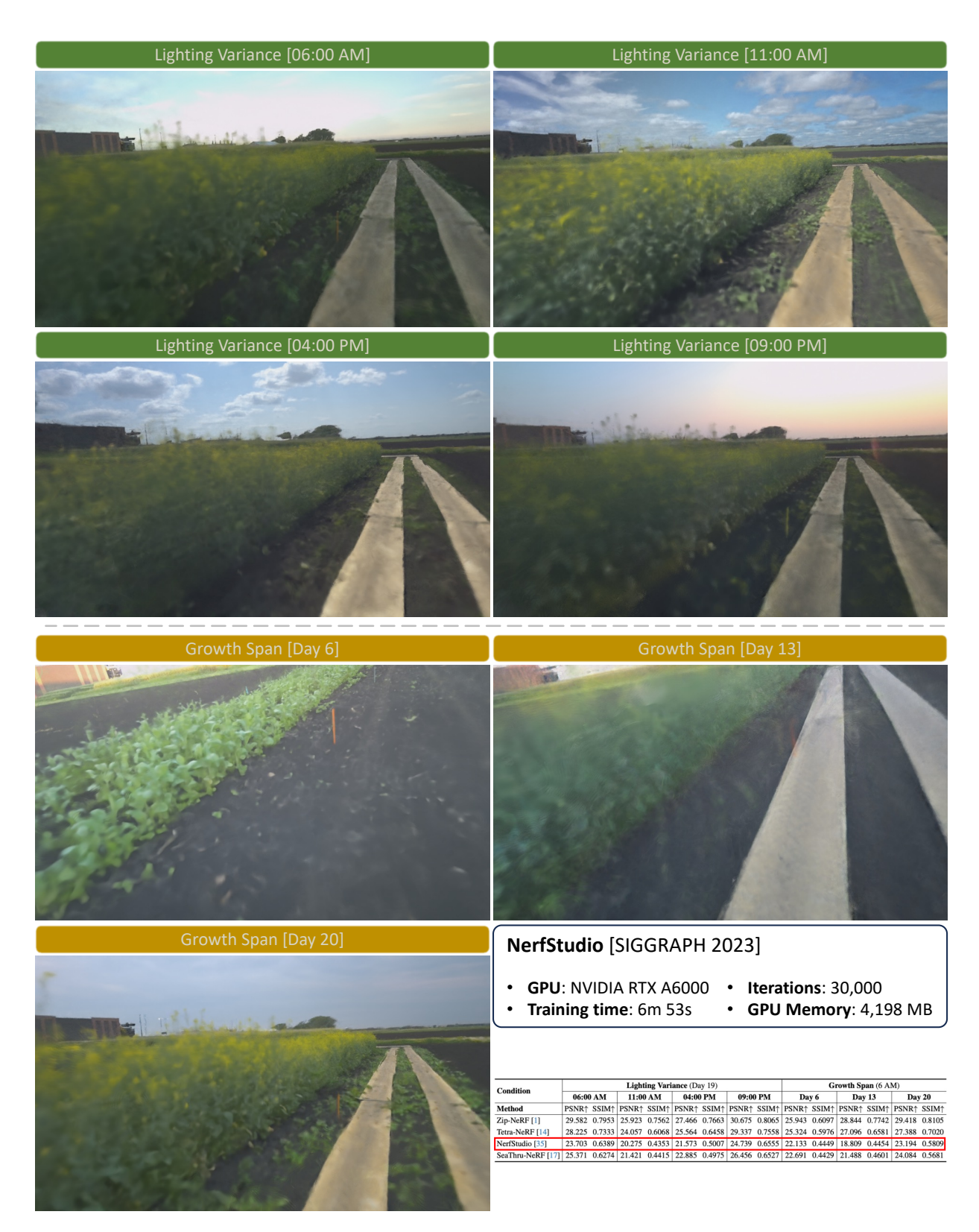


Figure 25. Qualitative Novel View Synthesis Results of NerfStudio [35]

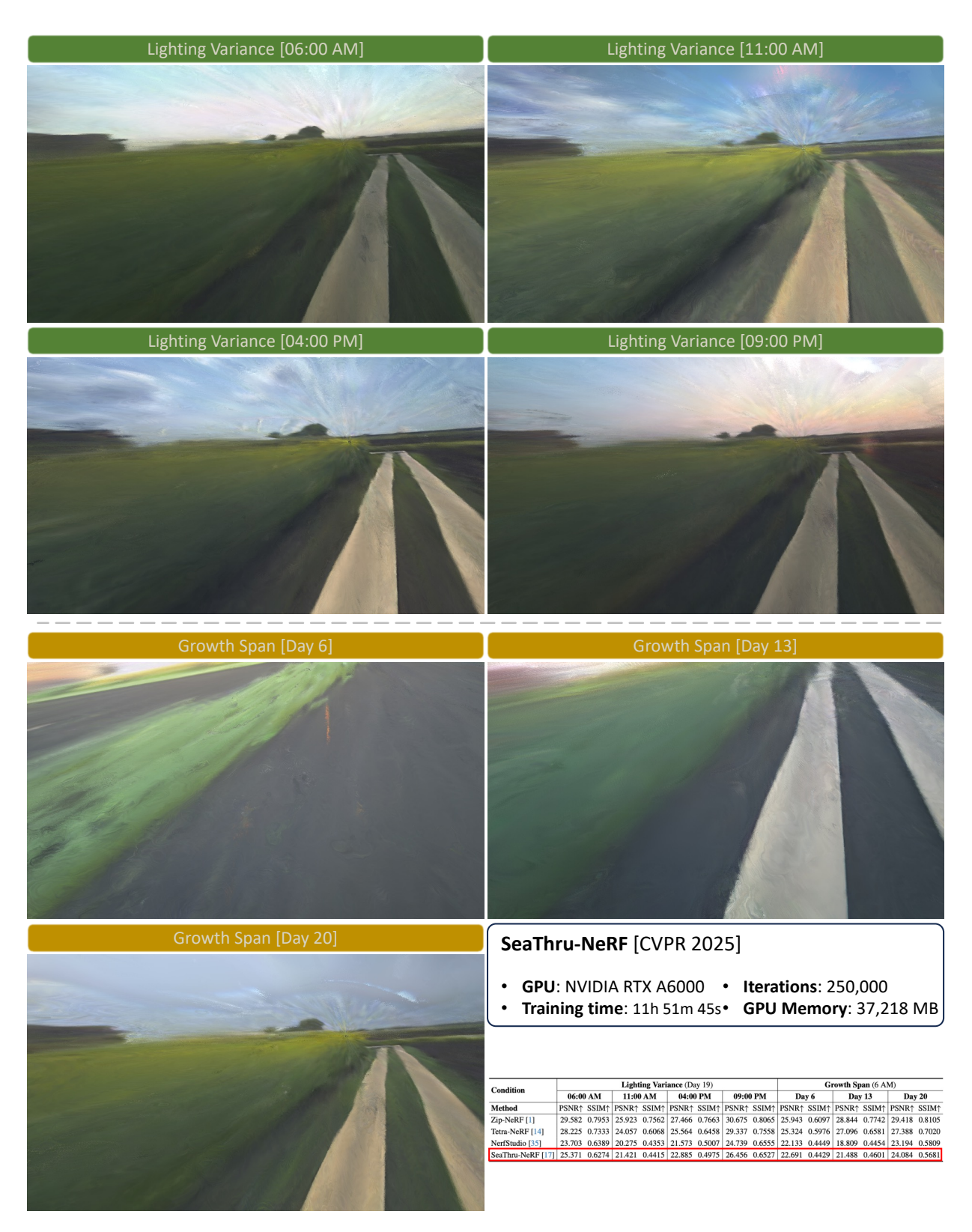


Figure 26. Qualitative Novel View Synthesis Results of SeaThru-NeRF [17]

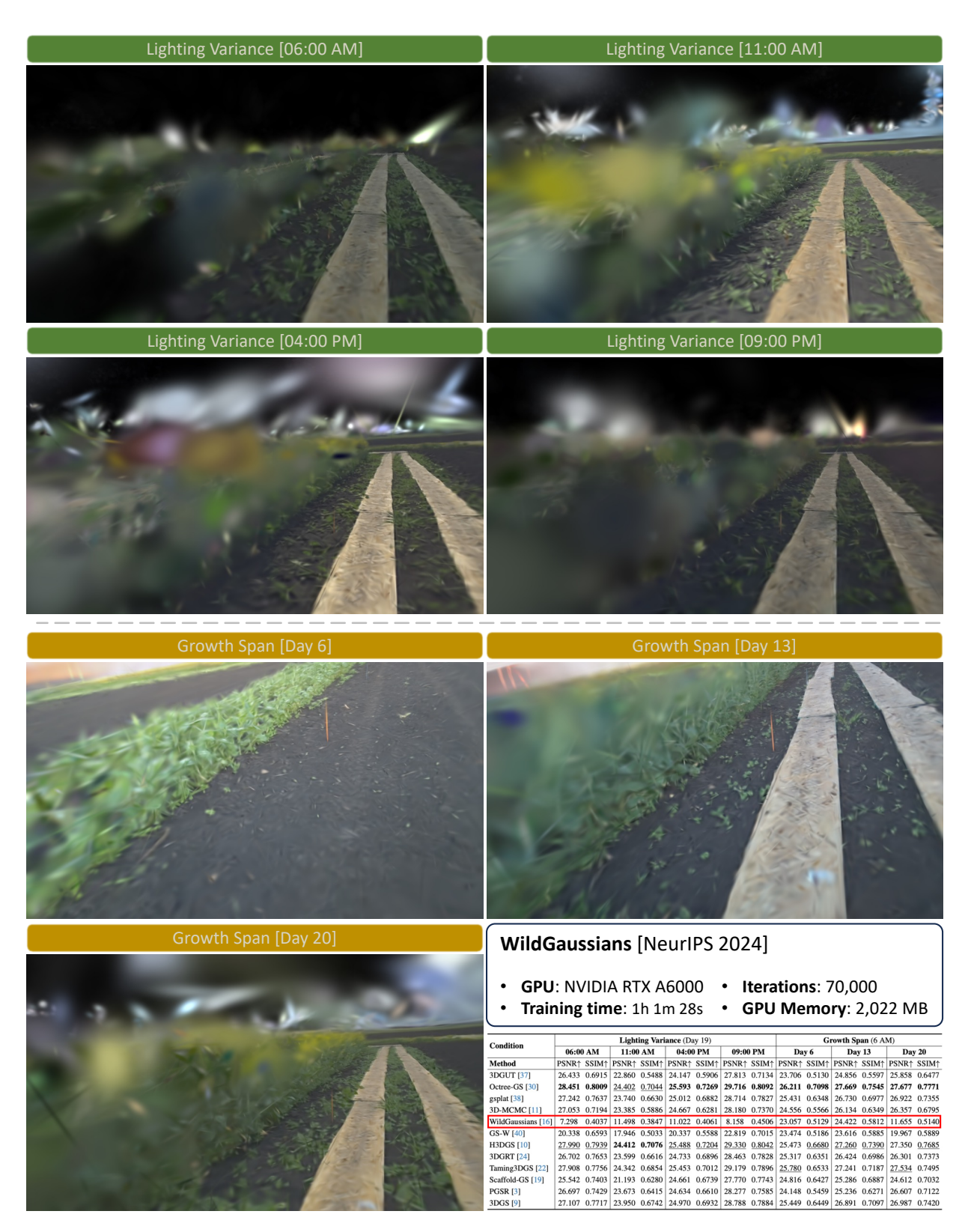


Figure 27. Qualitative Novel View Synthesis Results of WildGaussians [16]